UNIVERSIDAD DE COSTA RICA
GRADUATE STUDIES SYSTEM

RESOLUTION IMPROVEMENTS ON POLY(METHYL METHACRYLATE) AS ELECTRON-BEAM LITHOGRAPHY RESIST

Thesis submitted for consideration of the Graduate Studies Program in Physics Committee for the degree and title of Academic Master in Physics

JOSE PABLO ARRIETA NAVARRO

Rodrigo Facio University City, Costa Rica
2012

After climbing a great hill, one only finds that there are many more hills to climb.

- Nelson Mandela

Acknowledgments

To start, I want to thank Professors Karl K. Berggren and Henry I. Smith, for accepting me as a visiting student and believing in me during and after my visit. I will never be able to thank them enough; they pretty much flipped my horizon from that first acceptance reply (06/28/10) on.

I am immensely grateful with Vitor R. Manfrinato, for everything he did to help and guide me during and after my stay at MIT, he is a great colleague and friend I hope to work with him again in the future.

Furthermore, there are many people whose knowledge, patience, and guidance contributed to the completion of this work and for which they deserve my gratitude:

To Dr. Mark Mondol and Jim Daley for their great guidance and help during my stay at MIT. I had no time to learn things by myself so being able to clarify my doubts with them was just the thing I needed to accomplish my research goals.

To Dr. Leslie W. Pineda Cedeño for being an amazing surrogate advisor, never setting limits to my imagination and always encouraging my crazy ideas. On that note, I will also acknowledge the CELEQ for always backing my initiatives.

To Dr. Federico Muñoz for giving me the freedom of looking for my desired research field even when that meant something not investigated in Costa Rica, needing to file proposals and look for funding.

To Dr. Jose A. Araya Pochet for giving me the first opportunity to do research and allowing me to learn the efforts needed to do things right. More in specific for teaching me to

always double and triple check things at every step, this is something that has served me enormously throughout the years.

To the Microstructures Research Center, in specific its former director, Dr. Alberto Alape, for selecting my proposal for the 2012 research fellowship; which gave the first funding to the interference lithography project.

To Corey P. Fucetola and Samuel M. Nicaise for accepting to come to Costa Rica and share a bit of their knowledge on nanofabrication, also for their friendship, help and collaboration throughout the time.

To Faraz Najafi, and Lin Lee Cheong for helping me dream big even when my mental preconceptions did not allow me at the time.

To Dr. Yong-Ho Kim, Qingyuan Zhao, Lars M. Schonenberg, Donald Winston and everyone at the Quantum Nanostructures and Nanofabrication Group for their friendship and help.

Now on a personal note I want to thank my fiancée, Paola Rodríguez Marín, for these past five years, for enduring the hard times and enjoying the good ones, and for always believing in me; I am fortunate to have you.

Last but not least to my parents, grandparents, sister, and family in general for their continued encouragement and support. I can only hope that I will continue to make you all proud.

"Esta tesis fue aceptada por la Comisión del Programa de Estudios de Posgrado en Física de la Universidad de Costa Rica, como requisito parcial para optar al grado y título de Maestría Académica en Física"

Dr. Rodrigo Carboni Méndez
Representante de la Decana
Sistema de Estudios de Posgrado

Dr. Federico Muñoz Rojas
Director de Tesis

Dr. Karl K. Berggren
Asesor

Dr. Leslie W. Pineda Cedeño
Asesor

Dr. Jose A. Araya Pochet
Asesor

Dr. Jorge Gutiérrez Camacho
Director
Programa Posgrado en Física

Jose Pablo Arrieta Navarro
Candidato

Table of Contents

Abstract

The present thesis expands the topic of lithographic resolution improvement of poly(methyl methacrylate) (PMMA) as a positive tone electron-beam resist. The investigation used electron-beam lithography (EBL) to define sub-10 nm structures on PMMA.

Previous investigations obtained 25-nm-pitch dot arrays and 40-nm-pitch lines after AuPd pattern transfer. This thesis presents an improvement over these results, resolving 20-nm-pitch dot arrays and 34-nm-pitch nested L's structures after Au/Ti lift-off.15-nm-pitch isolated double-dot and triple-dot structures were resolved and helped to learn more about the resolution limits of PMMA as electron-beam resist. In addition, this research used calculations regarding proximity effect, contrast limitations, and intrinsic resist roughness to determine the factors currently limiting resolution. A manuscript with these findings is currently being prepared, with the candidate featuring as lead author.

The findings of this work were applied to collaborations on two separated areas of research: colloidal quantum dot placement and templating of protein assemblies. From the quantum dots placement collaboration a manuscript was already submitted for publication.

This last section of the thesis also explains other lithography-related work, in specific Helium-ion milling of graphene and low-cost experiments on interference lithography.

Resumen

En la presente tesis se expande el tema de mejora de la resolución litográfica del uso de poli(metil metacrilato) (PPMA) como material resistivo de tono positivo al haz de electrones. La litografía por haz de electrones (EBL) es utilizada para definir estructuras de tamaños menores a 10 nm en PMMA.

Investigaciones previas obtuvieron arreglos de puntos con una separación de 25 nm y arreglos de líneas con una periodicidad de 40 nm mediante transferencia de los patrones con AuPd. Esta tesis presenta una mejora sobre estos resultados, obteniendo arreglos de puntos con una separación de 20 nm y arreglos de L's anidadas con una periodicidad de 34 nm luego de *lift-off* de Au/Ti.

Estructuras aisladas de dos y tres puntos con una separación de 15 nm fueron obtenidas para ayudar a entender más acerca de los límites de resolución del PMMA como material resistivo al haz de electrones. Junto a esto, esta investigación usa cálculos relacionados a efectos de proximidad, limitaciones de contraste y rugosidad intrínseca del material resistivo para determinar los factores que limitan actualmente la resolución. Un manuscrito con los desarrollos de este trabajo se está desarrollando actualmente, figurando al candidato como autor principal.

Los desarrollos de esta tesis fueron aplicados a dos áreas de investigación separadas: el posicionamiento de puntos cuánticos y de arreglos de proteínas. De la colaboración en posicionamiento de puntos cuánticos, un manuscrito fue enviado a revisión a la revista Nano Letters. Esta última sección de la tesis también explica otros trabajos relacionados a litografía, en específico, el fresado de grafeno por iones de Helio y experimentos de bajo costo de litografía por interferencia.

List of Figures

Abbreviations List

_A	Ampere = Coulomb/second, SI Unit
_C	Coulomb, SI Unit
_m	meter, SI Unit
μ_	micro = 10^{-6} m
CD	Critical Dimension
CELEQ	Electrochemistry and Chemical Energy Research Center
CMOS	Complementary Metal-Oxide-Semiconductor
d_0	Base Diameter
D_0	Clearing Dose
D_i	Intrinsic Dose
D_t	Threshold Dose = 0.75 D_0
D_W	Working Dose, a multiple of D_0
e	Electron
EBID	Electron Beam Induced Deposition
EBL	Electron Beam Lithography
EECS	Electrical Engineering and Computer Science
f_	femto = 10^{-15}
GNR	Graphene nanoribbon
HIM	Helium Ion Microscope
HSQ	Hydrogen silsesquioxane
IPA	Isopropyl alcohol
k	Areal Dose Energy Contrast

k_	kilo = 10^{3}
LER	Line Edge Roughness
m_	milli = 10^{-3}
MIBK	Methyl isobutyl ketone
MIT	Massachusetts Institute of Technology
n_	nano = 10^{-9}
NA	Numerical Aperture
p_	pico = 10^{-12}
PL	Photoluminescence
PMMA	Poly(methyl methacrylate)
PSF	Point Spread Function
QD	Quantum Dot
SEM	Scanning Electron Microscope
STFE	Schottky Thermal Field Emitter
VHG	Variable holographic grating

Chapter 1. Introduction

1.1. Lithography

Lithography, from the Greek, λίθος -lithos- stone meaning and γράφειν -graphein- to write, is the method of using a mask, to make reproductions of an original pattern. The Hohokam tribe in the Southwest of the United States of America (USA) first developed this technique around the year 900 to 1150 AD, for shell decoration (Figure 1-1). In the western culture, Alois Senefelder first used lithography for printmaking in the year 1796. From that time on, lithography has been used in several areas, starting from the original paper printing to the more modern semiconductor industry.

Figure 1-1: Decorated shells from the Hohokam tribe in Southwest of USA, from 950 to 1150 AD; the first historic examples of lithographic techniques.

Lithography and more specifically photolithography is a technology ubiquitous in the semiconductor industry in which the planar fabrication process[1] reliably manufactures trillions of transistors every year.

1.1.1. Planar fabrication process

Industry and academia have used the planar fabrication process for over 50 years[2], developing vast amounts of techniques and processes. This section explains a subset of the fabrication techniques, also shown in figures 1-2 and 1-3.

The process starts with a clean Si wafer (Figure 1-2a) that has a native SiO_2 layer on top. A layer of photoresist is spun (Figure 1-2b) over the entire width of the wafer, to the desired thickness. Current production wafers have a diameter up to 300 mm and fit hundreds of dies on its surface, but the mask and illumination system expose just one die at a time. To avoid stitching errors the mask and illumination system need careful alignment (Figure 1-2c). After this alignment, the exposure step starts (Figure 1-2d). Exposure switches the dissolution rates of the exposed areas. In the case of positive resist, exposed areas become soluble in the developer (Figure 1-2e), dissolving the exposed volume until the substrate interface; whereas negative resist is originally soluble in the developer and therefore only exposed areas stay after the development.

Silicon wafers have a native SiO_2 layer on their surface, which inhibits the action of doping agents or the resistance of deposited contacts. SiO_2 etching removes this layer (Figure 1-2f) and promotes doping and contact adhesion by leaving behind a bare Si surface. At this point, there are two alternatives, the additive, or the subtractive processes, which as the name says, add or remove material from the wafer.

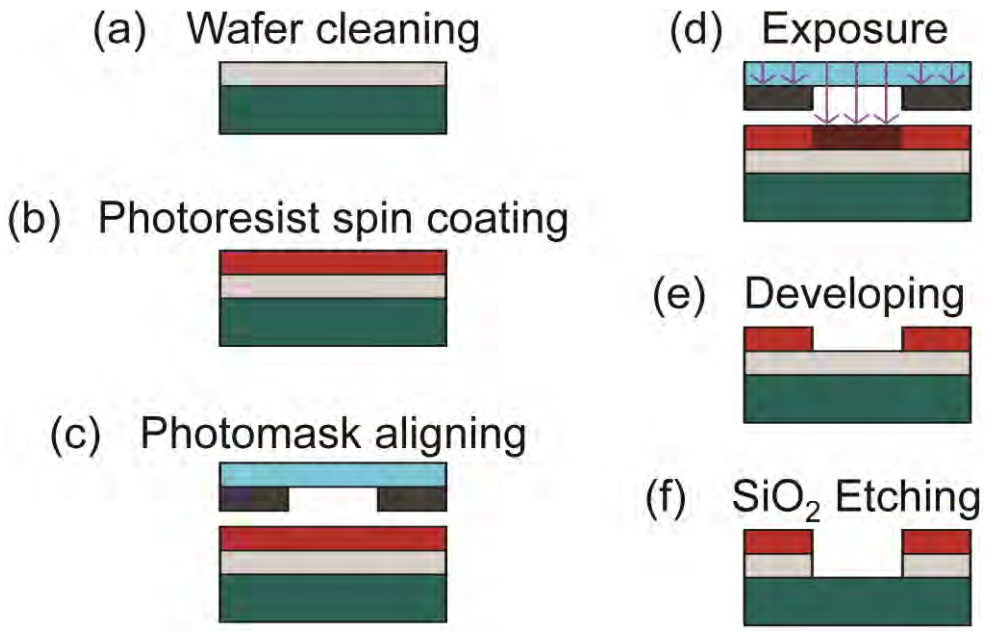

Figure 1-2: Schematic of the planar fabrication process. A clean wafer (a) is coated with a photoresist layer (b), following, a mask is aligned, (c) and an illumination source exposes the resist (d) changing its dissolution rate in exposed areas. A wet development process (e) removes the exposed resist (in the case of positive resist) and leaves the native SiO2 layer. Later an etching process (f) removes the SiO2 layer exposing the bare Si substrate. The process continues in figure 1-3.

The subtractive process, starts with the SiO_2 etching step (Figure 1-3a), followed by a Si etching process (Figure 1-3b) that removes only the bare Si, and makes a trench on the substrate. This process ends by using a solvent to remove the remaining photoresist in the wafer (Figure 1-3c), leaving behind the etched wafer.

Additive processes evaporate a material on top of the wafer (Figure 1-3d). This process can make contacts if the material is metallic or highly conductive; or dope the substrate by evaporating Si dopant materials (B, P, Ga, As, etc.) which change the conductivity of the exposed region. In the doping case, the substrate is annealed to guarantee uniform dopant diffusion inside the semiconductor. After the deposition, a lift-off procedure (Figure 1-3e) strips the deposited material/photoresist layer. If desired a further etching

procedure can be done to use the deposited material as a hard mask and leave behind risen structures (Figure 1-3f).

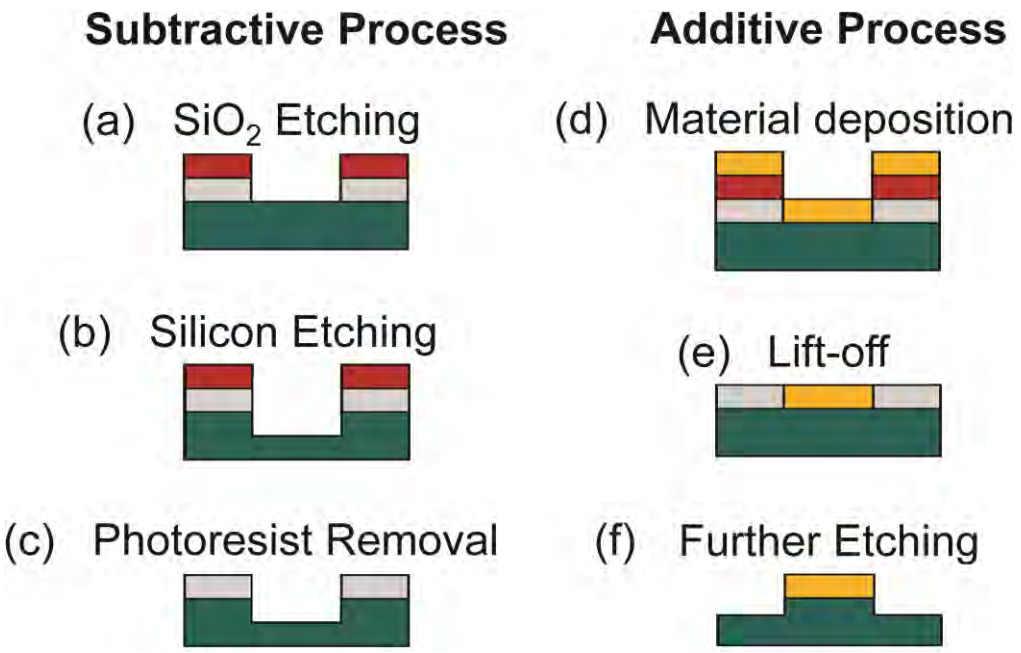

Figure 1-3: Schematic of subtractive and additive processes. The subtractive process starts with the SiO_2 etching step (a), to which follows a Si etching process (b) and ends with the photoresist removal (c) leaving behind a trench in the substrate. In the additive process after the SiO_2 etching (a), metal or dopants are deposited (d) and stripped by lift-off (e). Depending of the process, a further etching step follows (f). To fabricate a desired device a combination of these steps needs to be followed.

The manufacturing of an actual integrated circuit needs to follow dozens of additive and subtractive processes, to comply with the requirements of the circuit designers and process engineers.

The continual improvement of the planar fabrication process has enabled the extraordinary advances of the computer industry (memory, density, processor speed, etc.) for the last 50 years. This reduction enabled the development of Moore's law[3] (Figure 1-4), the empirical and economical law that states that transistor count in an integrated circuit doubles roughly every two years, scaling down the transistor area by 50% during that period. In this

way, transistor count has gone from 2300 in 1971 to 2.6 billion in 2011 integrated circuits (Figure 1-4b). During this time, the critical dimensions (CD) have shrunk from 10000 nm in 1971 to 25 nm in the present dies, a reduction of 400 times (Figure 1-4a) over 40 years.

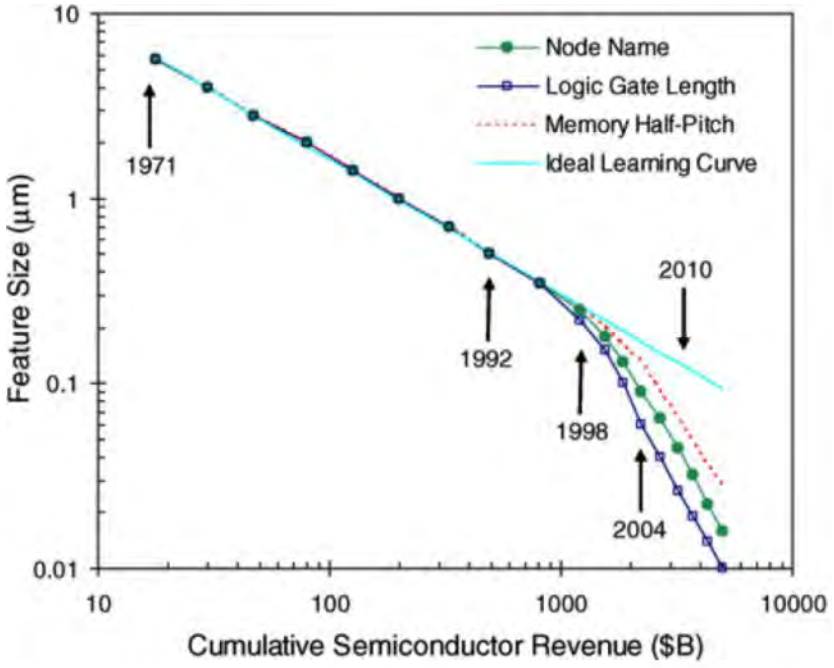

(a)

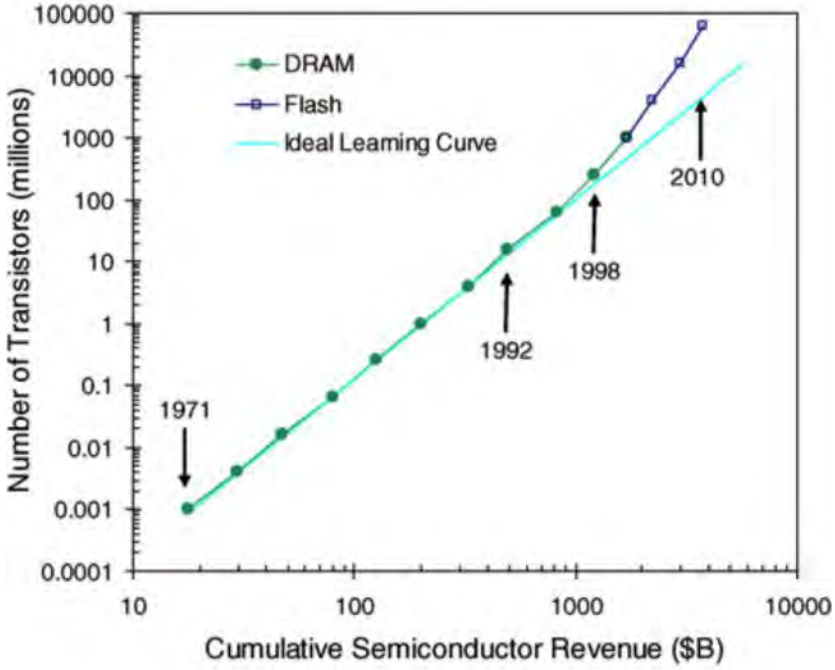

(b)

Figure 1-4: Economical representation of Moore's Law. (a) shows transistor feature size and (b) number of transistors per die as a function of cumulative semiconductor revenue. Each figure shows representative years of production. Taken from reference 3.

In specific, the processes explained previously represent several of the techniques used in photolithography, having a mask and an optical illumination source. Nonetheless, different lithographic technologies use analogous techniques and processes.

1.1.2. Terminology

There are several terms referring to resolution and lithographic feature sizes. Figure 1-4 shows in a visual way these different terms by depicting a transversal image of a typical complementary metal-oxide-semiconductor transistor (CMOS) transistor.

The pitch represents the distance between identical features in an array, in the case of figure 1-5 it represents the distance between the drain and source contacts. In the same line, half-pitch is one-half of the pitch value. Finally, the critical dimension (CD) is the smallest resolvable feature in the design. This thesis will use the terms critical dimension and feature size interchangeably.

In a photolithography system, the critical dimension is estimated prior to the exposure by taking the formula: $CD = k_1\lambda/NA$. Where λ is the wavelength of incident illumination, NA is the numerical aperture of the optical system, which is proportional to the refractive index of the lens/substrate interface. The k_1 factor refers to process-related factors; its value is physically limited to 0.25 but commercial apparatus work around 0.4.

Using a single exposure system 29.9 nm features were resolved in 2006 by IBM[4] using a fluid with a 1.64 refractive index in the lens/substrate interface and quartz crystal (n

= 1.67) at the end of the lens. The smaller features attainable for the 32 nm node onwards have been possible by double exposure / double etch processes.

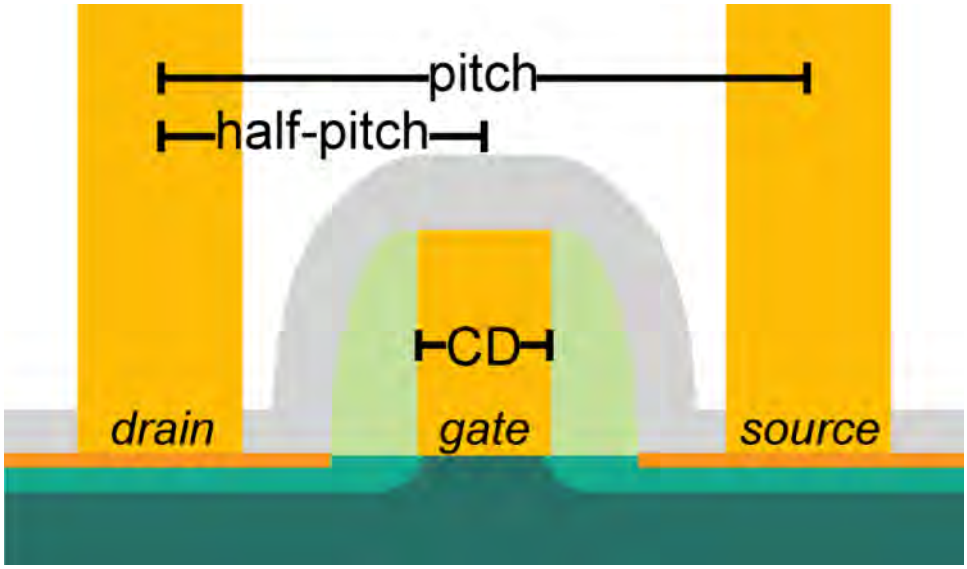

Figure 1-5: Cartoon of the cross-section of a CMOS transistor. The figure visually marks the different terms used in lithographic resolution investigations.

1.2. Electron-beam lithography

The techniques explained previously were projection based, transferring patterns from a mask to expose selectively areas on a wafer. There are several direct write lithography alternatives, between them: electron-beam lithography (EBL)[5], direct-write laser lithography[6], probe-based lithography[7] [8], and zone-plate-array lithography[9] are some of most widely used.

First proposed as a lithography alternative in 1959 [10] [11], EBL is now widely used worldwide. This maskless technology is the one investigated in the present thesis.

EBL uses a standard scanning electron microscope (SEM) column with a Schottky thermal field emission (STFE) source. The more relevant modifications needed by a SEM column to do lithography are an electron beam blanking system, an arbitrary pattern

generator, and ideally a sub-10 nm precision stage controller. The addition of active vibration isolators and passive acoustic isolators help improve resolution and stochastic lithography errors. Figure 1-6 shows the essential parts of an EBL.

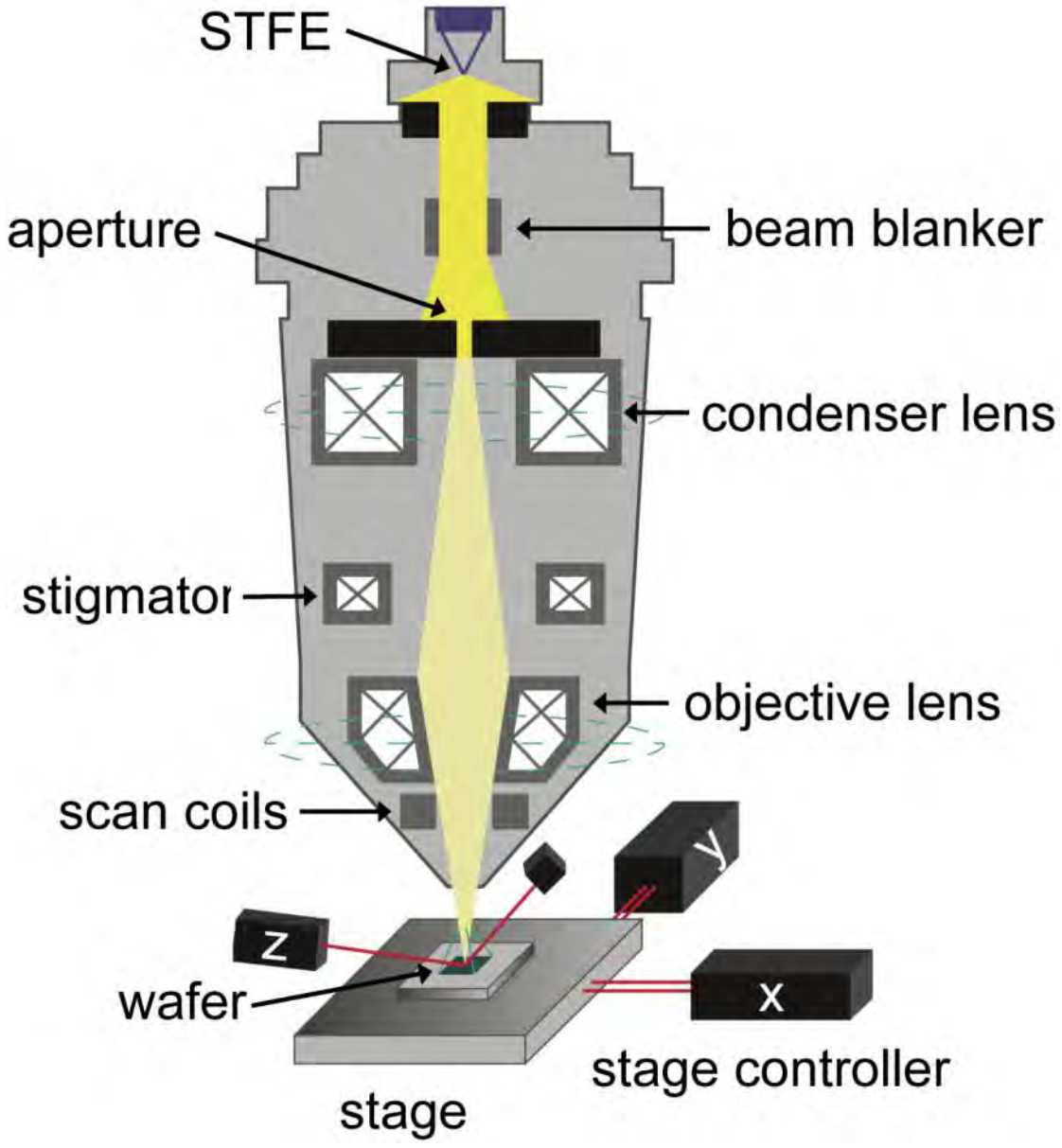

Figure 1-6: Schematic diagram of a scanning electron-beam lithography system, similar to the one used in the research shown in this thesis. The system comprises a SEM column with modified scanning coils controllers for improved pattern generation, an e-beam blanking system for dose control, and a stage controlled by laser interference to avoid major stitching problems.

1.2.1. Electron-beam energy transfer

High-energy electrons penetrating into a solid material collide with atoms and electrons surrounding an atom. Depending of the type of collision, the incident electron might conserve its energy (elastic scattering) or 'share' it with the material (inelastic scattering). These scattering processes limit the resolution of the lithographic technique, broadening the effective area of the spot size. Figure 1-7 depicts the different scattering processes.

There are two types of elastic scattering. Forward scattering is the most frequent event and is the case in which electrons deviate from the beam center axis and the electrons are directed through the substrate. This process broadens the beam's spot size and therefore limits the maximum resolution. Furthermore, the amount of forward scattering is dependent on the resist layer thickness with less scattering on thin layers and more in thicker ones.

Backscattering is the process in which electrons recoil after a collision reversing its momentum normal to the substrate. This process happens primarily when electrons try to enter the Si wafer, which has a higher atomic density. Backscattered electrons travel long distances in the resist and therefore are more likely to generate inelastic scattering events; depositing energy in the resist. This scattering event provides a background dose at large area patterns and can limit the resolution for high-density large-area patterns.

Secondary electron emission is the primary inelastic scattering event. These electrons are emitted when incident electrons share part of their energy to an electron in the resist. These secondary electrons have a smaller amount of energy than the incident ones and therefore spend more time in the resist breaking polymer bonds.

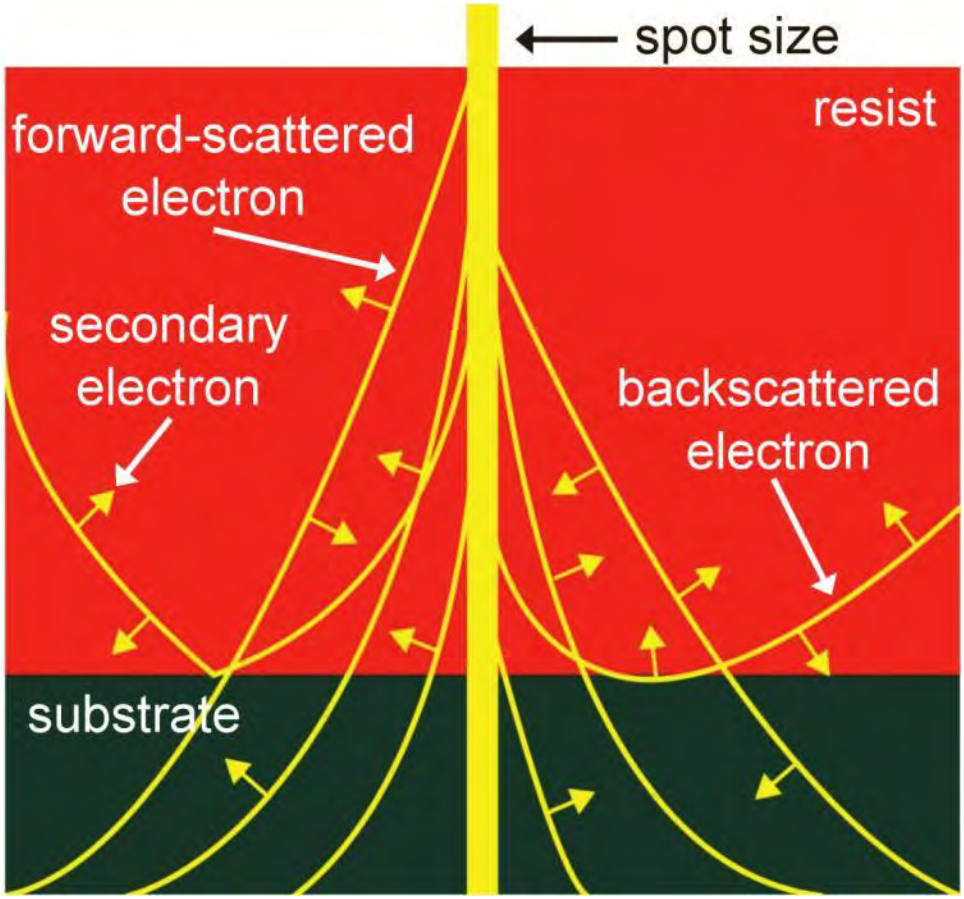

Figure 1-7: Schematic illustration of the resist exposure process. The incident electron beam interacts with the resist generating elastic collisions, in form of forward and backscattering events, and inelastic collisions, which generate secondary electrons. Inelastic collisions are in charge of the exposure process, by depositing energy and leading to molecular scission and polymer crosslinking. Backscattered electrons contribute to long-range proximity effects.

1.2.2. Point Spread Function

It is possible to quantify the energy deposition at a certain distance of a written EBL pattern. The Point Spread Function determines how the electron-beam deposits energy in the resist[12]. This function is dependent on the EBL system settings and on the resist layer thickness.

Figure 1-8 shows the point spread function (PSF) for 40 nm thick positive and negative poly(methyl methacrylate) (PMMA) lithographic processes[13]. There are two definite regimes in the figure, at sub-100 nm distances, forward scattering dominates and has a Gaussian behavior, and at over 100 nm distances, backscattering dominates and the function decreases much more slowly giving the added exposure dose when writing large-area high-density patterns. The relevant data for this thesis is the one for positive tone PMMA and in specific the sub-100 nm PSF data. Please refer to reference 12 for further discussion on PSF.

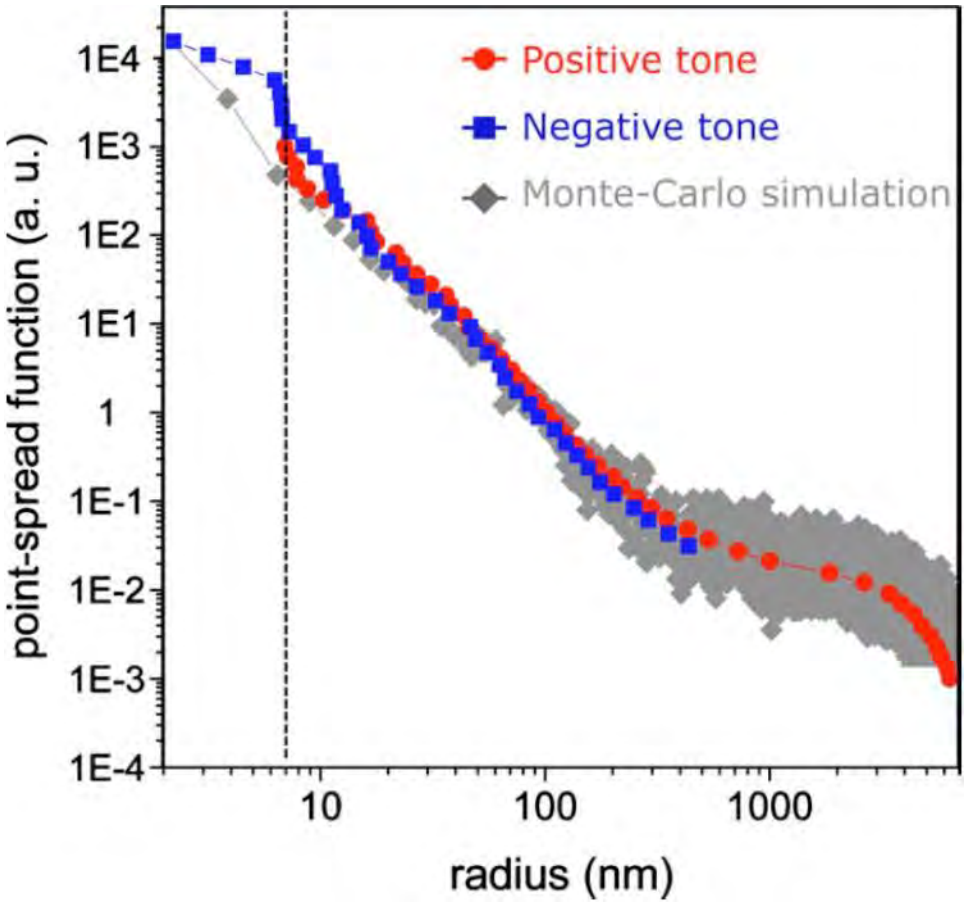

Figure 1-8: Point spread function measurements for 40 nm thick PMMA. The figure shows the PSFs of positive and negative tone PMMA as well as Monte-Carlo simulations of the PMMA layer and exposure process. Extracted from reference 13.

1.2.3. Resist Exposure

Polymer bond breaking is the cause of resist exposure, which happens in two ways: chain scission and polymer crosslinking. In chain scission, the secondary electron hits the polymer structure (Figure 1-9) and separate the long polymer chain in smaller portions, oligomers, which are more soluble in the developer than the original structure. This is the principal process that happens on a positive tone resist, such as PMMA or ZEP-250a.

Polymer crosslinking is a different process in which incident electrons, separates polymer chains, but instead of making soluble oligomers, the broken chain-ends attach to other polymers making an insoluble network. In negative resists, like hydrogen silsesquioxane (HSQ) and calixarene, the original molecule is small and soluble in the developer. Crosslinking turns this small soluble molecule into an insoluble network that stays after the developing process.

Crosslinking and chain scission are processes that happen on any polymer. Dosage, polymer characteristics and developing parameters determine the final behavior as a lithographic resist, i.e. PMMA can act as a positive or negative resist, depending on the dose and development conditions.

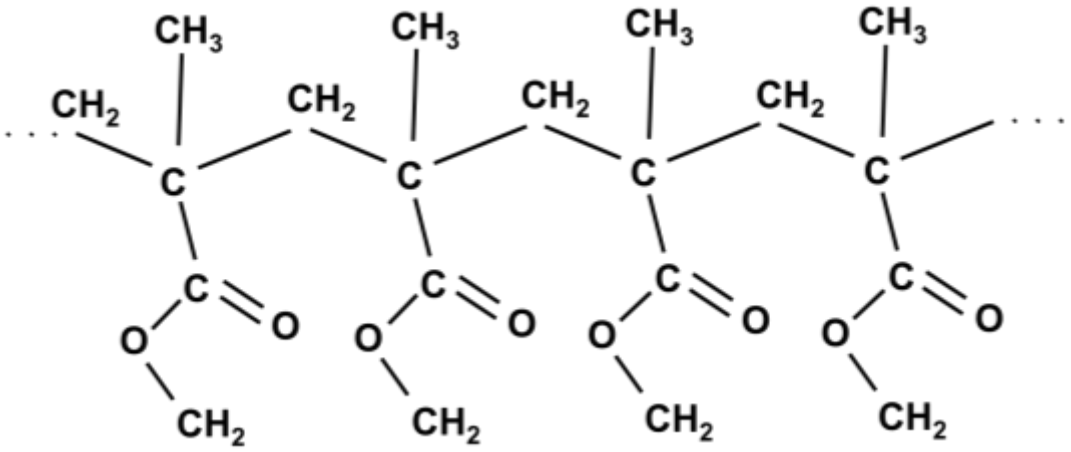

Figure 1-9: Line diagram of PMMA molecular structure. Molecular scissions separate long polymer chains into soluble oligomers. Crosslinking bridges and binds polymer chains together leaving an insoluble polymer network. PMMA is a dual tone resist, where both processes happen in parallel.

1.2.4. Resolution Improvement

A series of variables relating to EBL system specifications and resist/sample processing determines the maximum resolution of the process. In terms of the EBL system specifications, resolution depends on the acceleration voltage, beam spot size, beam jitter, beam current, flare, working distance, source filament, stigmation, focusing, step size, proximity effect correction, aperture size, pattern design, and others.

From the resist side, molecular weight and distribution, impurities, solvent used, resist concentration, spin thickness, baking temperature, baking system (oven, hot plate), substrate material, base monolayer coating, ultra violet / ozone etching, reactive ion etching, wafer handling, storage, cleaning, cleaving, developer composition, rate, contrast, temperature and, agitation, as well as others factors limit the attainable resolution.

Careful control and continual optimization of these variables is the only way of achieving resolution improvements. The particulars of this process optimization are the content of the present thesis.

References 14, 15, 16, 17, and 18 give further information on lithography and nanofabrication technologies and processes.

1.3. Aims and Goals

Electron-beam technologies are able to resolve sub-10 nm features. Electron-beam-induced deposition (EBID) is able to resolve sub-1 nm features and 5 nm pitch line

patterns[19] by using organometallic gas precursor decomposition, a process, which requires large doses. EBL is capable of resolving sub-10 nm pitches[20] [21]„ and features sizes as small as 1 nm[22] by using HSQ, a negative tone resist with dose over 1000 times lower than with EBID[23].

Sub-10 nm resolution EBL, has emerging applications on templated self-assembly[24] [25], nanoelectronic devices[26] [27], bit-patterned media[28] [29], and mask manufacturing for nanoimprint lithography[30] [31].

In the case of PMMA, a positive tone resist, and in specific the first resist used in EBL[32], several studies have worked towards determining its resolution limits[33] [34] [35] [36] [37] [38]. These resolution limits are higher than with HSQ, set at 25 nm pitch dot arrays and 40 nm pitch lines and spaces both etched through a AuPd layer [34]. 30 nm pitch dot arrays, and 20 nm lines and spaces were resolved after Ni lift-off[37]. In the case of isolated structures, 3 nm wide lines[35] [37] and sub-5 nm dots[33] are attainable with PMMA. Furthermore it was determined that cold development[39] and high temperature baking[33] (> 200°C) help to improve resolution for this resist.

Independently of the possibilities of negative tone resists such as HSQ or calixarene, there are many applications that need a positive-tone resist capable of achieving sub-20 nm pitch resolutions, these applications include nanoscopic light antennas[40] [41], plasmonic nanostructures[42] [43], and single-quantum dot or 1D nanostructure placement.[44] [45] [46].

This project investigates the minimum resolvable pitch in PMMA for several pattern geometries, not minimum feature size that requires a different process optimization. Furthermore, it uses calculations based on contrast curve data, PSF, and line edge roughness (LER) to determine the constraints that PMMA faces to improve resolution even further.

Chapter 2. Methodology

The goal of resolution improvement required the use of several process optimizations. In specific, the adjustments used were cold development[39], thin resist, different baking temperatures[33], patterning of isolated structures, and Au/Ti lift-off.

2.1. Sample Processing

44 ± 1 nm thick layers of PMMA were spin coated on top of Si (001) wafers. The PMMA resist had a 950 k molecular weight, was dissolved in anisole, and was supplied by MicroChem Corp. Samples were then oven baked at 175°C or 225°C for 5 min to evaporate remaining solvents and in the case of 225°C, to decrease surface roughness[33].

2.2. Pattern Writing

Exposures were done on a Raith 150 EBL system[47]. The specifications used were: 30 kV acceleration voltage, 20 μm aperture, 150 pA beam current, 50 μm write field, 1 nm step size, 6 mm working distance, and 5 μs settling time. Careful stigmation and focusing was needed.

The dose ranged from 1 fC/dot to 197.8 fC/dot in dot structures and from 0.1 nC/cm to 19.7 nC/cm on line structures, there were 30 dose increments done per structure written. The development of structures was done in 3:1 isopropyl alcohol : methyl isobutyl ketone (IPA:MIBK) solution for 30 s and 3 development temperatures were used depending on the sample: 6°C, -5°C, and -15°C in order to determine the ideal temperature to resolve these structures[39].

The designs written were isolated patterns, in order to work in a forward-scattering limited regime. In specific the patterns written were 6 by 6 double dot structures (Figure 2-1a), 6 by 6 triple dots structures (Figure 2-1b), 10 by 10 dots arrays (Figure 2-1c), and nested L's structures (Figure 2-1d).

All these structures are high density but isolated from any other feature. This fact decouples the influence of backscattered electrons in resolution improvement, an important and relevant feature of this research. Lastly, all patterns written were single pixel dots or single pixel lines to decrease feature size as much as possible.

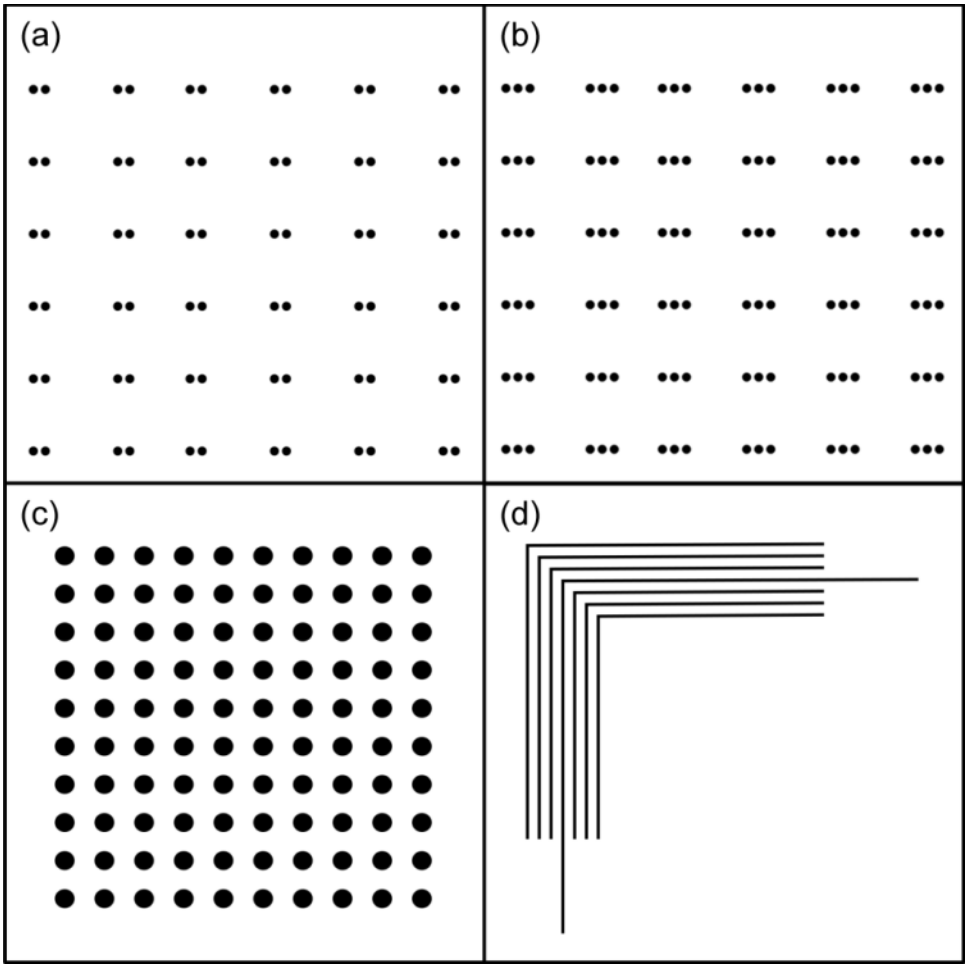

Figure 2-1: Schematic diagram of the different isolated patterns used in this investigation. (a) 6 by 6 double dot structures, (b) 6 by 6 triple dot structures, (c) 10 by 10 dot array, and (d) nested L's. Each double and triple dot structures are isolated 250 nm from neighboring structures.

The design of the double and triple dots structures separates each two/three dots a distance of 250 nm from the next closest structures. This separation guarantee, for the case of 15 nm pitch double dots that the background dose one dot perceives due to the writing of the other dot is 200 times larger (calculated) than the dose perceived from writing all the other dots in the 6 by 6 double dot array. Furthermore, by separating the patterns by 250 nm from neighboring structures, only forward-scattering processes limit the resolution and sharpness of the final structure.

2.3. Metrology

The investigation used a Raith 150 as a SEM for metrology. The settings used were 20 kV acceleration voltage, 30 μm aperture, and 6 mm working distance. The metrology was limited using bare PMMA due to e-beam induced charging and morphing, which showed the need for an improved metrology strategy, in this case a lift-off procedure.

The lift-off procedure consisted in the e-beam evaporation of a layer 3 nm of Ti and 7 nm of Au. Following this, acetone dipping, striped the excess metal and PMMA layers of the samples. This procedure left behind the Au/Ti layer only in completely resolved areas, which had complete removal of the PMMA layer, therefore leaving a bare SiO_2 surface for Au/Ti adhesion. This helps assure that measurements done were of fully resolved structures something that it is not possible to do when using bare PMMA or metal layer deposition metrology.

2.4. Resolution Analysis

The analysis used feature size measurements at different pitches and doses, to determine the variations of its values and better understand resist behavior. Furthermore, for better determining the resolution limits and its constraints, the analysis used PSF, contrast curve measurements, as well as LER calculations. Chapter 3 explains the findings of these analyses.

2.5. Overview

Figure 2-2 depicts a summary of the overall lithography process explained previously. The process starts with a clean wafer, on top of which a 44±1 nm thick layer of PMMA is spin coated and then baked (Figure 2-2a). A Raith 150 EBL system does the exposures generating soluble oligomers in the exposed areas (Figure 2-2b). Samples are developed in 3:1 IPA:MIBK for 30 s (Figure 2-2c). A 3nm layer of Ti and 7 nm layer of Au is evaporated on top of the sample (Figure 2-2d). Acetone immersion strips the metal and resist layer, which leaves behind the patterned metallic structures (Figure 2-2e). Sample imaging on a Raith 150 SEM gives a contrast similar to Figure 2-2f on which the metallic dots show a clearer contrast due to higher secondary electron emission yield. The two metrology strategies used in this thesis are bare PMMA metrology (Figure 2-2c) and lift-off metrology (Figure 2-2e).

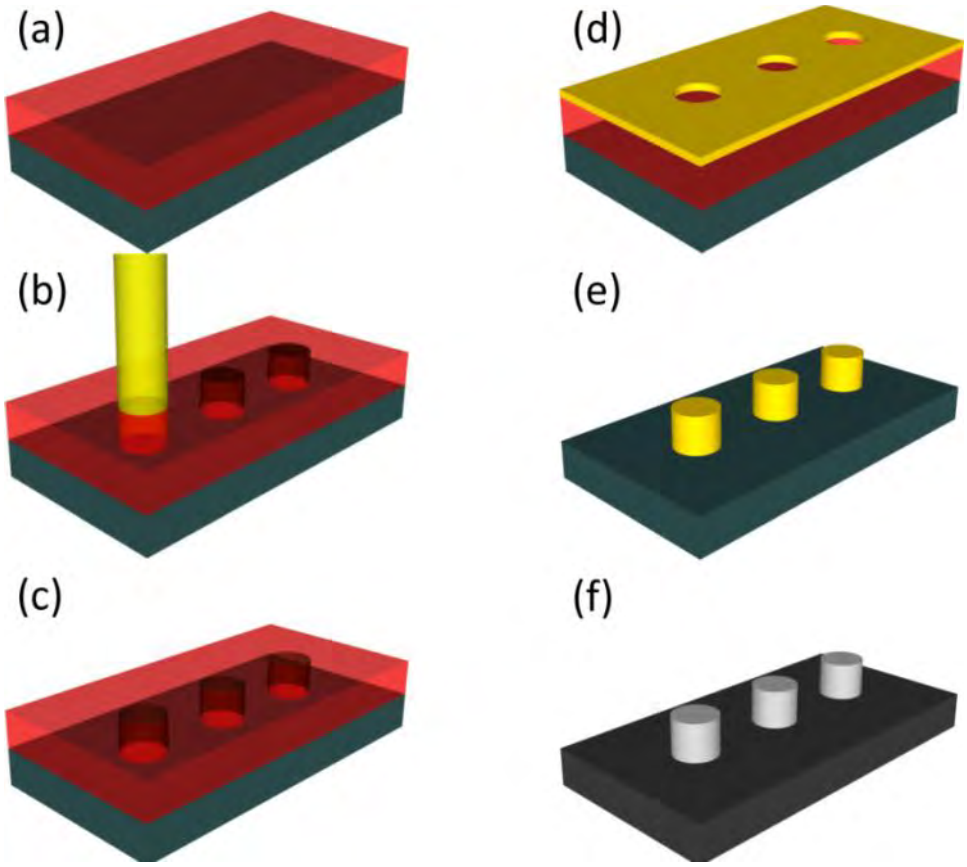

Figure 2-2: Schematic diagram of the lithography procedure for the different metrology strategies followed on this thesis. The process starts with a PMMA coated Si substrate (a), then e-beam writing (b) exposes the PMMA. Samples are developed in 3:1 IPA:MIBK for 30 s (c). On bare PMMA metrology, the sample is image on this stage. For lift-off metrology, a 3 nm Ti and 7 nm Au layer is e-beam evaporated (d). Later acetone lift-off (e) strips the PMMA and Au/Ti layers. (f) depicts a representation of the imaging process showing the contrast between metallic posts and the semiconductive substrate.

Chapter 3. Results

3.1. Metrology

PMMA is a carbon based material and therefore when imaged on SEM, charging and morphing of structures was expected. This considered, promising results were obtained when imaging bare PMMA, resolving 23 nm pitch double dot structures (Figure 3-1a), 30 nm 10 by 10 dots arrays (Figure 3-1c), and sub-4 nm diameter features (Figure 3-1d).

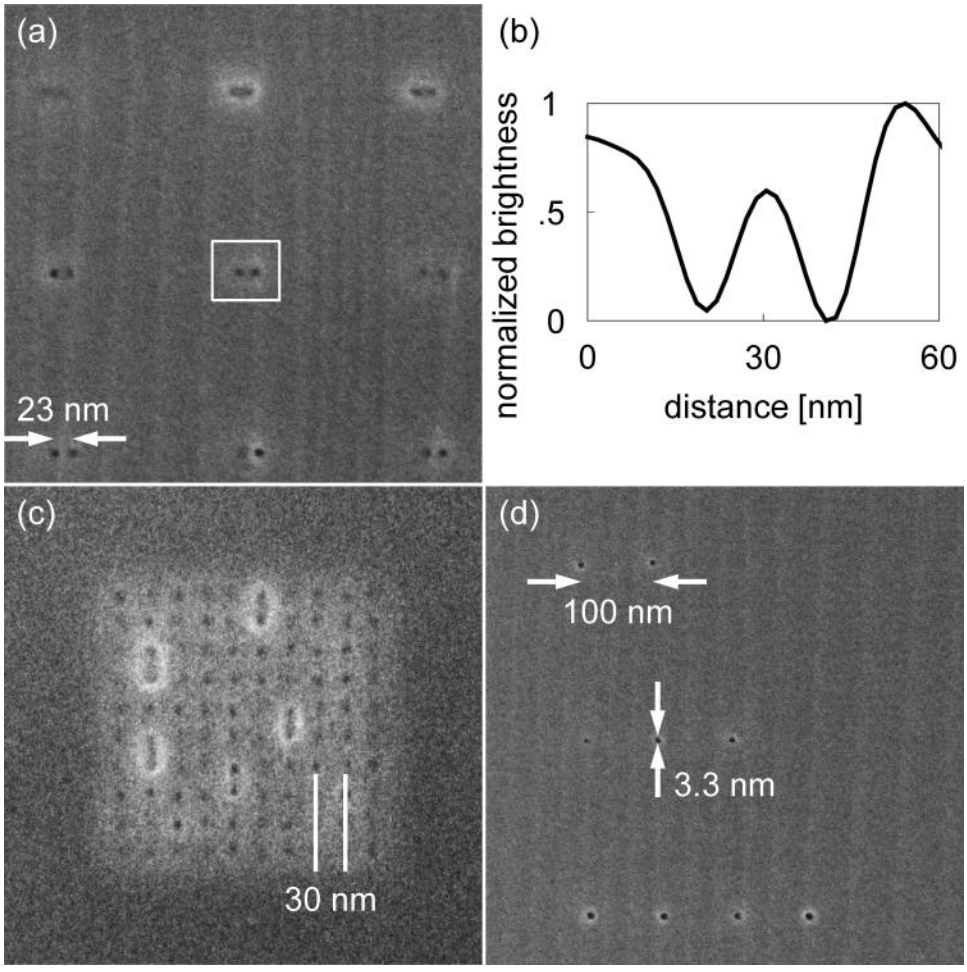

Figure 3-1: Resolution limits obtained after bare PMMA metrology. (a) 23 nm pitch double dots, (b) line grab of the double dot structure framed on (a), (c) 30 nm pitch 10 by 10 dot arrays, (d) sub-4 nm features on 100 nm pitch structure. All these structures were oven baked for 5 minutes at 225°C, and

developed in 3:1 IPA:MIBK for 30 s at 6°C. Vertical stripes on (a) and (d) are due to scans over the area done before capturing the micrographs. The differences in contrast in (c) were expected to be due to local resist fluctuations.

Lower pitches and smaller feature sizes need higher magnification, which in turn give higher areal dose on the imaged area. Because of resist morphing at higher magnification, we chose a different metrology strategy for lower pitch structures. Metal evaporation helps to improve contrast nonetheless; due to nonuniformities of metal e-beam evaporation, an added structural uncertainty in this process.

This experiment employed Au/Ti lift-off because of several benefits obtained. Au/Ti lift-off metrology restricts imaging to only fully resolved features, which are the ones that clear the PMMA layer completely and allow metal adhesion to the Si substrate. Additionally, structures imaged are resilient towards electron-beam exposure and thus higher contrast, more stable and averaged measurements are possible.

Results for Au/Ti lift-off showed that 20 nm pitch dot arrays (Figure 3-2a), and 34 nm pitch nested L's (Figure 3-2d) were resolvable. In addition 15 nm pitch double dot structures (Figure 3-3a), with a yield of 51% and 15 nm pitch triple dots structures (Figure 3-3c) at a yield of 32% were resolved. Figure 3-2c shows 32 nm pitch nested L's, which are almost resolved but show some pattern collapse.

At the resolution limit, an increased variability in feature size is present, shown in Figures 3-2b, 4-3b, and 4-3d, which can be one of the culprits of the low yield of these structures. In contrast, at higher pitches, a lower variability and higher yield, is obtained as shown in Figures 4-2b, 4-2d 4-3b and 4-3d.

At 15 nm pitch, double and triple dots structures have a pitch 40% smaller than previous results[33], in the same way the somewhat larger 20 nm pitch 10 by 10 dots arrays represents a 20% improvement over previous values. Line structures show a decrease in pitch of 15% when compared to literature[34]. These represent the latest of a long line of incremental developments on the use of PMMA as e-beam resist; a material for which resolution limits have been sought for since its first uses for EBL in 1968[32].

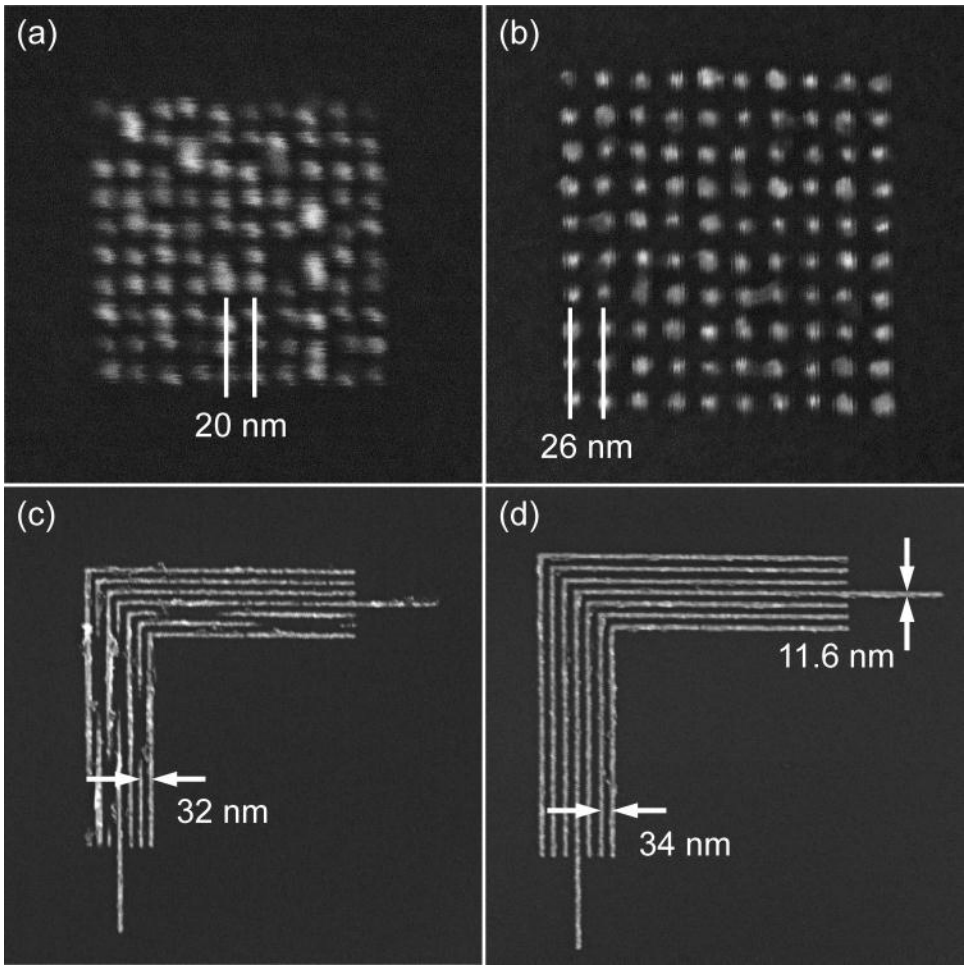

Figure 3-2: Resolution limits obtained for dots arrays, and nested L's structures after 3 nm Ti, 7 nm Au acetone lift-off. (a) 20 nm pitch dots array, (b) 26 nm pitch dots array, (c) 32 nm pitch nested L's, and (d) 34 nm pitch nested L's. All the structures were oven baked at 175°C and developed at -15°C for 30 s. The figures on the left show larger variability of feature size compared to the larger pitch structures on the right.

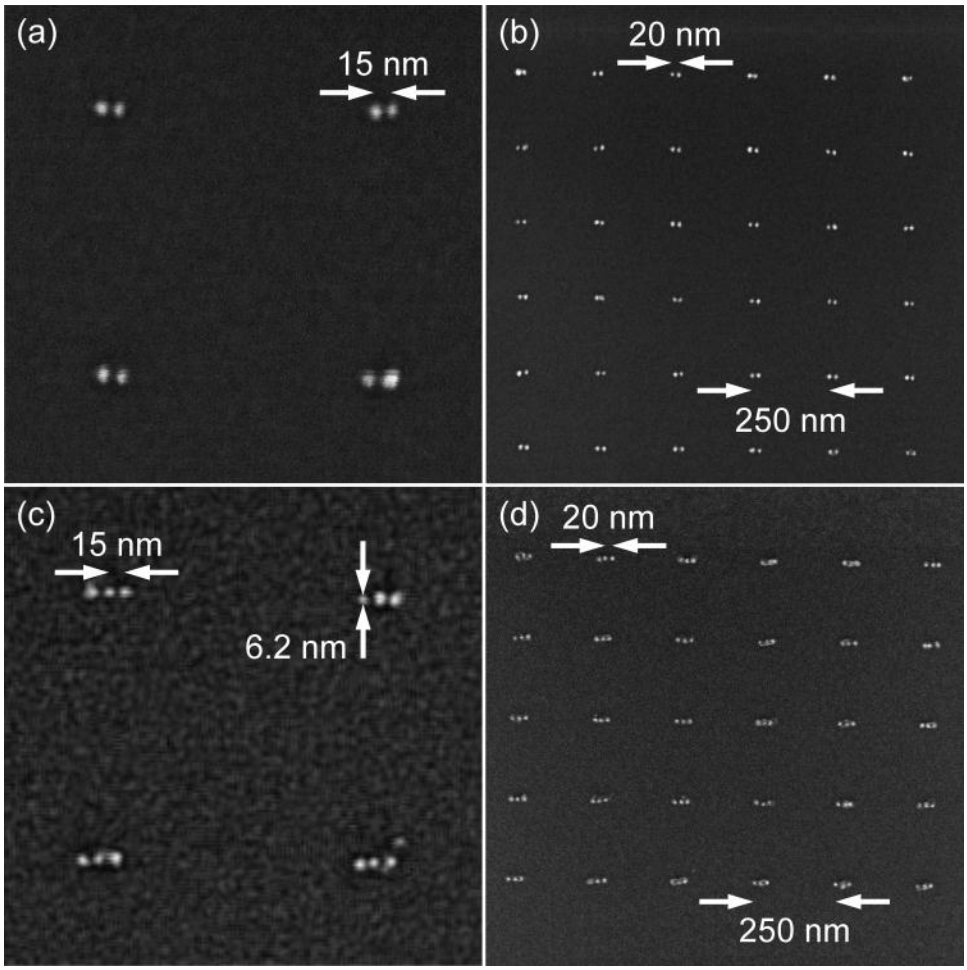

Figure 3-3: Resolution limits obtained for double and triple dots after 3 nm Ti, 7 nm Au acetone lift-off. (a) 15 nm pitch double dots structures, developed at 6°C. (b) 20 nm pitch high yield double dots structures, developed at -5°C. (c) 15 nm pitch triple dots structures, developed at 6°C. (d) 20 nm pitch high yield triple dots structures, developed at 6°C. All structures were oven baked at 225°C. The figures on the left show larger variability of feature size compared to the larger pitch structures on the right.

3.2. Areal Dose Energy Contrast

Deposited energy due to neighboring exposed structures generates the so-called proximity effect, which all structures written by EBL experience in some manner. Therefore, when writing features, the dose modulation, which determine the dose profiles in the resist is not completely sharp and commensurate due to long-range contributions from backscattered

electrons, and short-range effects due to forward-scattering events. The purple curve in Figure 3-4 shows a dose modulation profile for a 10 nm pitch double dot structure, using the PSF information from Figure 1-8. It is clear how there is a maximum dose, D_{MAX} precisely in the point the two dots were written but also in between the two dots there is a non-negligible dose, D_{MIN}, which depending on the closeness of the features can be high enough to expose the resist and make the features unresolvable. Section 3.3 will explain the other curves in Figure 3-4.

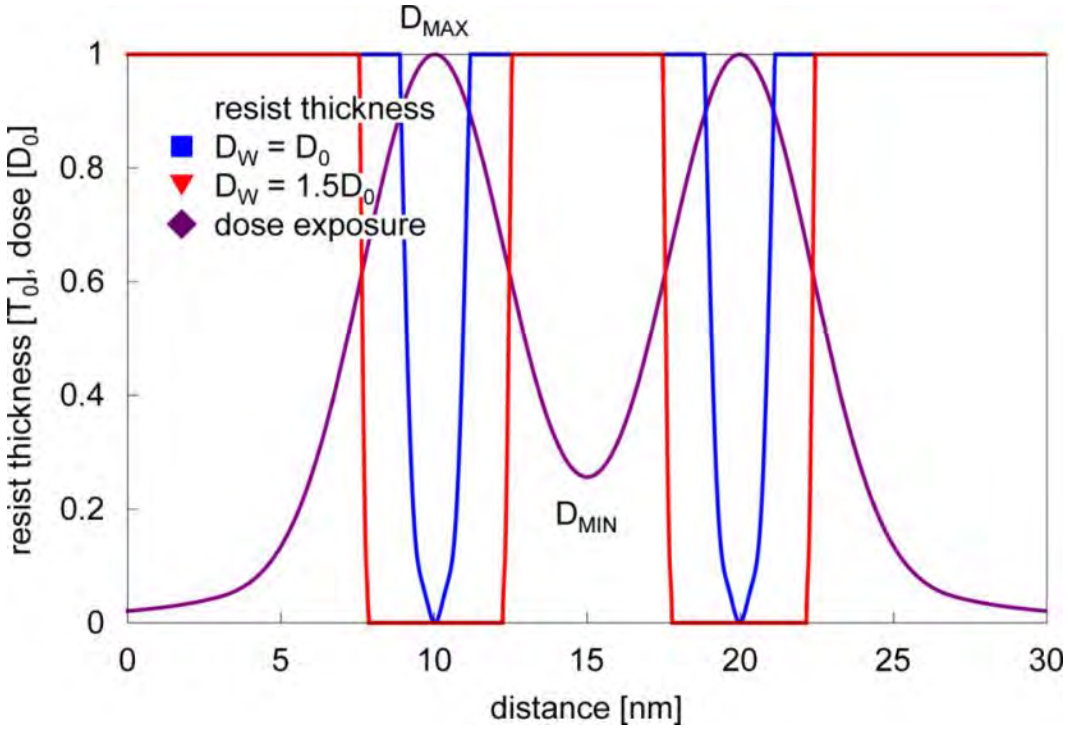

Figure 3-4: Profiles of dose modulation (purple) and calculated resist profiles for $D_W = D_0$ (blue), and $D_W = 1.5D_0$ (red) for 10 nm pitch double dots structures. D_0 is the clearing dose, needed to dissolve the resist layer completely, and D_W represents the dose used for the exposure calculations. In the blue curve, only the precise location written clears all the way through, making a conical shaped dot, not resolvable by lift-off, whereas the higher dose red curve predicts clearing a rod-like structure. D_{MAX} represents the dose in the precise location written whereas D_{MIN}, gives the minimum dose between written features. The relative value of the two will help to determine the contrast resolution limits in section 3-3.

PSF measurements done in a similar process[13] allow quantifying how resolvable a written feature might be. By calculating the areal dose energy contrast [48] $k = (D_{MAX}-D_{MIN})/(D_{MAX}+D_{MIN})$, it is possible to calculate the relative sharpness of the dose profile at a given pitch and structure, equating for beam characteristics and proximity effect contribution from neighboring structures.

Figure 3-5 shows the areal dose energy contrast calculations for all the structures written as well as large area dots arrays (10^6 dots). In the figure, the markers indicate the experimental resolution limits and the calculated areal dose energy contrast at that pitch.

These results exhibited an 85% areal dose energy contrast threshold value at the experimental resolution limit of all written structures. Decreasing this threshold, by improving processing, could lead to increased resolution. In addition, using a smaller spot size might aid in maintaining profile's sharpness even at lower pitches making it conceivable to think of future resolution improvements.

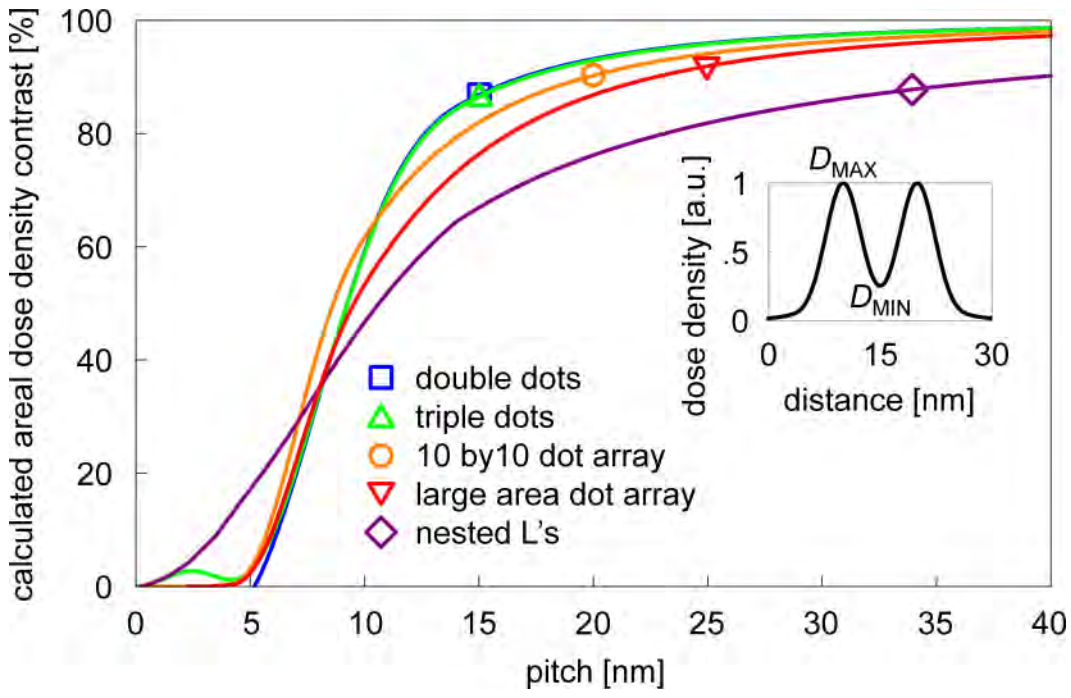

Figure 3-5: Calculation of the areal dose energy contrast as a function of pitch, $k = (D_{MAX} - D_{MIN})/(D_{MAX} + D_{MIN})$, for double dots (blue), triple dots (green), 10 by 10 dot array (orange), large area dot array (red), and nested L's (purple). Experimental resolution limits for each structure are marked on the curves. For all the resolved structures, the areal dose energy contrast was higher than 85%. The inset shows a dose modulation curve for 10 nm pitch double dots structures; it is clear from this how D_{MIN} gives a non-negligible dose to the resist due to proximity effects.

3.3. Resist Contrast

The performance of any photoresist can be characterized by its contrast curve. The contrast curve describes the remaining resist fraction of a uniformly exposed as a function of dose.

Figure 3-6 shows two PMMA contrast curves. The blue curve shows the contrast curve for 160 nm thick PMMA resist developed at 5°C[39]. With this curve it is possible to extrapolate the contrast curve for a 44 nm thick layer of PMMA (purple curve), according to Reference 49.

The threshold dose, D_T, represents the dose needed to remove 25% of the resist thickness; it is lower than the clearing dose, D_0, which is the one needed to dissolve the resist layer completely. In the case here investigated, it was determined that $D_T \approx 0.91 D_0$. Any dose higher than that value was considered high enough to completely expose the resist.

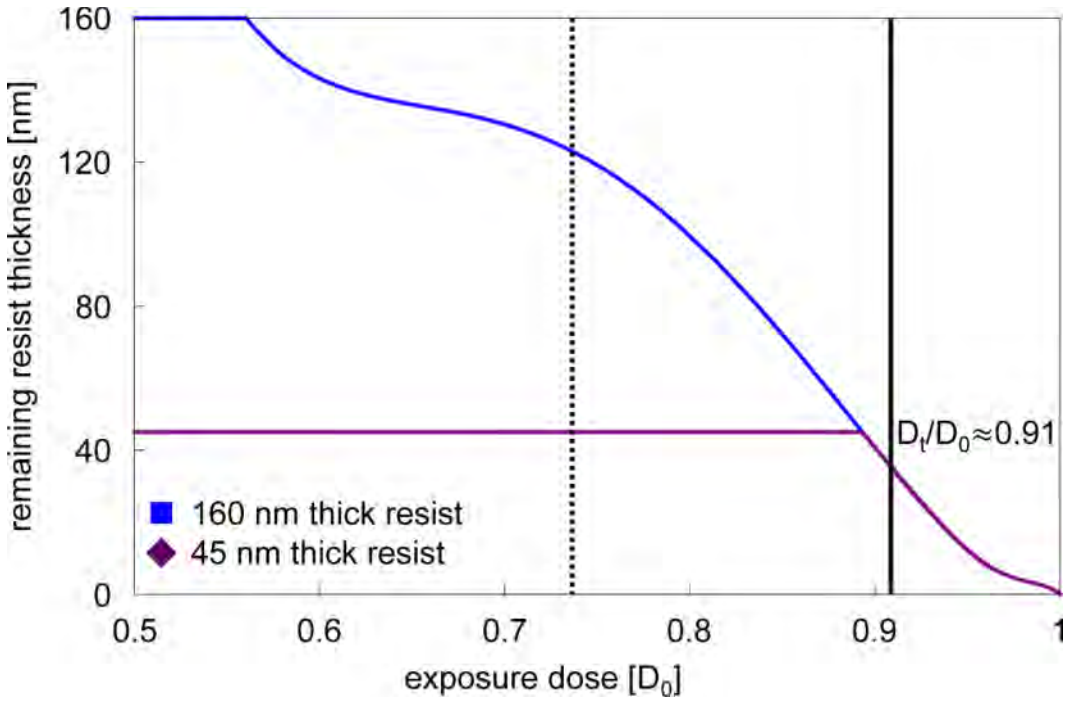

Figure 3-6: Contrast curve for PMMA at 5 °C for 160 nm thick resist layer (blue) and extrapolated contrast curve for 44 nm thick resist layer (purple) in units of clearing dose (D_0), showing a calculated threshold dose, $D_T = 0.91D_0$. The information on this figure was extracted from reference 39.

In a lithographic process, the working dose, D_W, which is the dose given at each exposure point, needs to be larger than D_0. The reason why is shown in Figure 3-4, on which the blue curve shows the resist profile for a $D_W = D_0$, it is clear how this profile has a conical shape and will not endure any pattern transfer process, i.e. lift-off. Applying a higher dose generates a rod-like profile, like the case on the red curve in Figure 3-4, which calculates the effects of $D_W = 1.5D_0$, this structure is capable pattern transfer. Higher doses will continue to generate rod-like structures but the radius of the dots will be larger, expanding as a function of this working dose.

Considering all this, it is possible to calculate a resolution limit due to resist contrast. This limit is set at the pitch value at which $D_{MIN} = D_T$ (Figure 3-4) any pitch lower than that

will have a proximity effect contribution high enough to expose the resist completely making features unresolvable.

Figure 3-7 shows a calculation of D_{MAX}/D_{MIN} as a function of pitch for all studied structures. In this figure, the horizontal dotted line represents the contrast resolution limit. This line represents the point in which $D_{MIN} = D_T$ for the case of doing an exposure with $D_W = 1.5D_0$ and shows that for all the structures studied, a resolution of 7.5 nm is conceivable. Consequently, from a resist contrast point of view, PMMA is still capable of enduring higher resolutions.

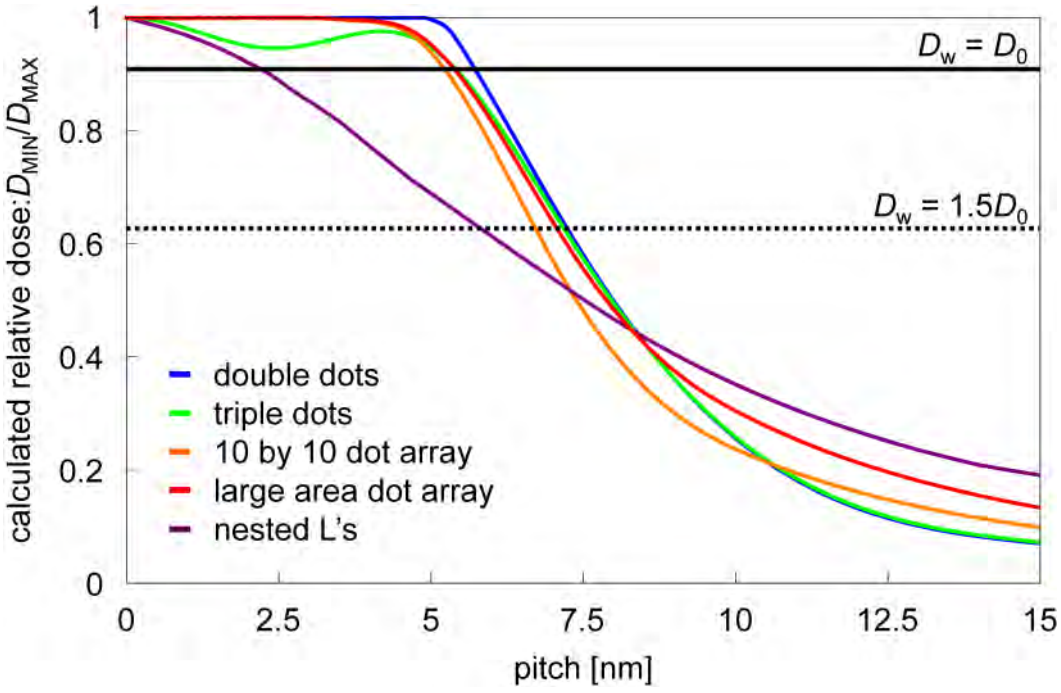

Figure 3-7: Calculation of the PMMA resolution limits due to resist contrast. The value was set by the pitch at which the $D_{MIN} = D_T$. Depending on the writing does, D_W, used, the maximum pitch attainable varies. The dotted horizontal line determines the resolution limit for $D_W = 1.5D_0$, whereas full line determines the one for $D_W = D_0$, Calculations were done for: double dots (blue), triple dots (green), 10 by 10 dot array (orange), large area dot array (red), and nested L's (purple).

3.4. Feature Size Variation

Previous analysis showed a clear route for improving resolution on PMMA, giving only processing and beam spot size as resolution constraints. Nonetheless, line-edge roughness and feature-size variation can limit further developments.

Figure 3-8 shows the progression of feature size standard deviation for double dot structures as a function of pitch. This data shows that the value at 15 nm pitch is almost 3 times larger than the value at 250 nm pitch.

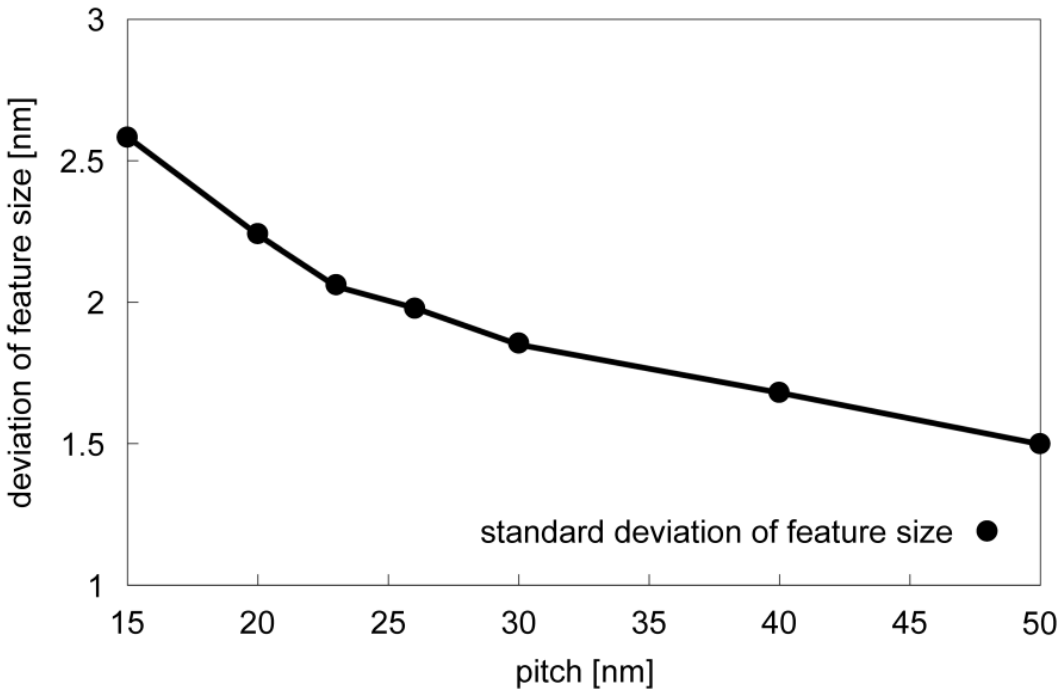

Figure 3-8: Feature size standard deviation versus pitch for double dot structures. It values grows as pitch is lowered giving a limitation for resolution improvement. At 250 nm pitch the standard deviation is 0.87 nm whereas at 15 nm pitch the value is 2.58 nm almost three times larger.

Figure 3-9 shows the experimental threshold dose and merge dose of double dots structures as a function of pitch. The figure shows how the difference in these doses (process window) decreases greatly when going to smaller pitches. In specific, this process

window goes from 43.9 fC/dot at 50 nm pitch to just 0.6 fC/dot or about 3600 electrons at 15 nm pitch. This lower process window can be the reason why lower pitches generate larger feature size variability and lower yielding structures. Section 4.5 will explain the meaning of the black line in figure 3-9.

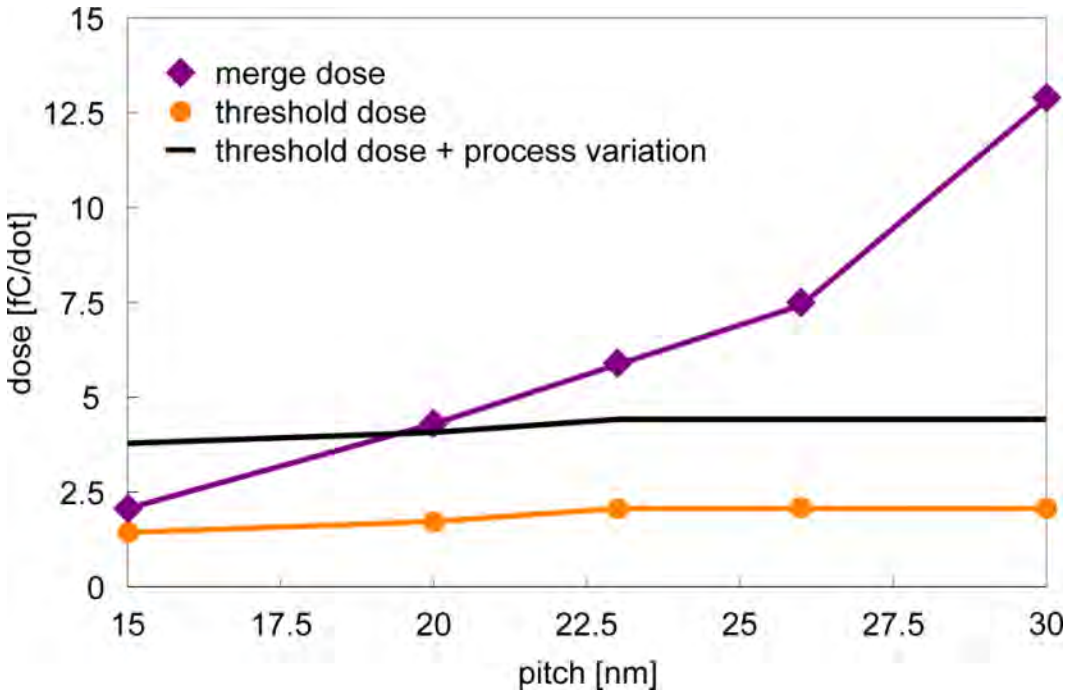

Figure 3-9: Threshold dose (circles), and merge dose (diamonds) versus pitch for double dots structures. The processing window is much smaller at lower pitches. The solid line represents the threshold dose plus the intrinsic process variation (D_i = 2.34 fC/dot), this value is higher than the merge dose for pitches lower than 20 nm and helps explain the larger variability at those pitches.

3.5. Intrinsic Process Variation

We evaluated the effect of PMMA feature size variation on resolution, by assuming that the feature size standard deviation at 250 nm pitch, σ = 0.87 nm, is due mainly to intrinsic resist roughness, a resist characteristic relatable to LER.

To quantify this, an intrinsic process variation (in units of dose) was determined, by fitting the feature size versus dose curve of 250 nm pitch dots arrays (Figure 3-10) and using

the feature size of 16 fC/dot exposed structures as the base diameter (d_0). The difference in doses that make the feature size to be $d_0 \pm \sigma$ equals $2D_i$. Where D_i= 2.34 fC/dot is the intrinsic process variation, as assumed, due to intrinsic resist roughness This value is larger than the process window at sub-20 nm pitches which generates the increased feature size variation. We can expand this to other low-pitch structures, with small processing windows, that make them to dose changes, making this a major resolution-limiting factor.

As an added visualization, the black curve of Figure 3-9 shows the experimental threshold dose plus this intrinsic process variation. It is evident how the curve exceeds the merge dot value for sub-20 nm pitches.

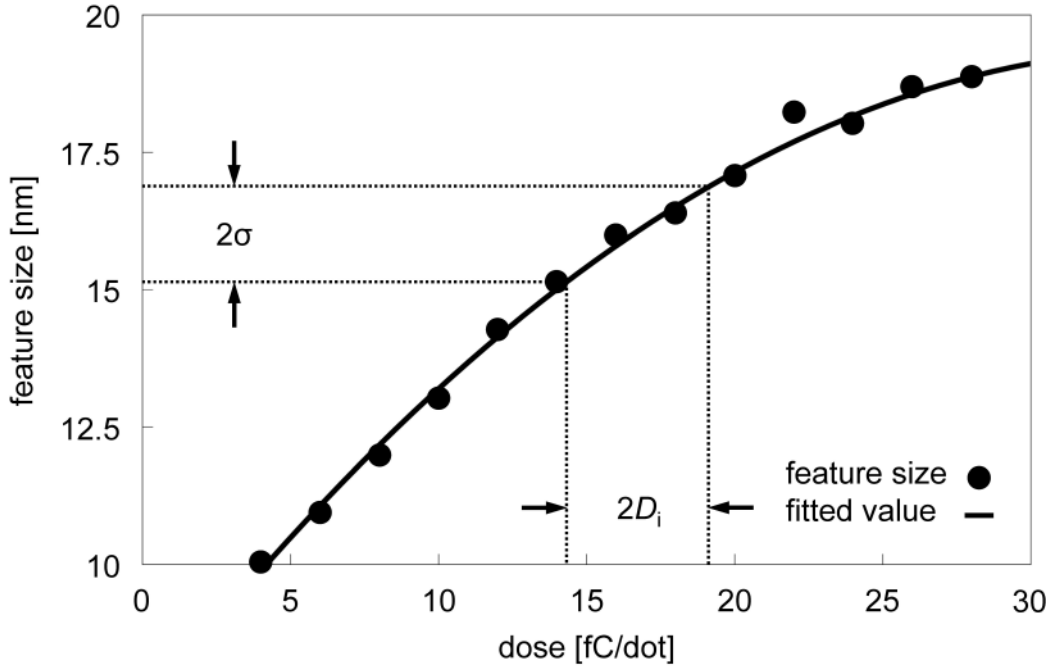

Figure 3-10: Experimental feature size versus dose for 250 nm pitch dots arrays. Taking the average feature size at the 16 fC/dot dose as the base diameter, d_0, the intrinsic process variation is calculated as half the difference in doses that give the diameters of $d_0+\sigma$ and $d_0.-\sigma$, where σ = 0.87 nm is the standard deviation for 250 nm pitch dots. This calculation gives an intrinsic process variation of 2.34 fC/dot.

3.6. Discussion

This thesis investigated the resolution limits of PMMA as a positive tone e-beam resist, as well as an assessment of the factors currently limiting this resolution. By doing Au/Ti lift-off, 15 nm pitch double dots and 34 nm pitch nested L's were resolved. These values are lower than literature[34 37] but larger than the expected contrast resolution limit of 7.5 nm pitch calculated by contrast curve and PSF measurements.

Using the data from figure 3-5 it is calculated that resolving 7.5 nm pitch features, will need an areal dose energy contrast value of 40%, which is a long way from the current 85% threshold. In the same note, by fitting the trends of feature size standard deviation of figure 3-8 for 7.5 nm pitch features, a standard deviation of ±3.4 nm is expected. This represents 45% of the actual pitch, clearly making it unfeasible to resolve these structures.

These two values depict the need for a processing and exposure change to guarantee increased resolution in the future. A sharper PSF will allow increasing the areal dose energy contrast at sub-15 nm pitches to values closer to the current experimental threshold. Additionally, improved sample processing, driven towards lowering the intrinsic resist roughness, will help foster future resolution improvements.

Chapter 4. Conclusions

The present thesis studied isolated structures written by EBL on a Raith 150 system. The features were designed to minimize backscattering contributions. In specific, 23 nm pitch double dots, and sub-4 nm features were resolved and imaged on bare PMMA metrology. Furthermore Au/Ti lift-off metrology, showed improved resolution, and 20 nm pitch dot arrays, 34 nm pitch nested L's structures, and 15 nm pitch isolated double and triple dot structures were resolved.

Calculations based on PSF and contrast curves showed an 85% areal dose energy contrast threshold and a calculated resolution limit due to contrast and proximity effects contribution lower than 7.5 nm pitch for all structures studied.

Process latitude measurements estimate an intrinsic process variation of 2.34 fC/dot. This value is larger than the process window for sub-20 nm pitch double dot structures. This helps to understand why sub-20 nm pitch structures have a lower yield and higher feature size variation when compared to larger pitch structures.

Considering the past conclusions it is determined that intrinsic process variation (related to LER), and finite spot size of the beam are the current constraints of PMMA resolution. Improvements in sample processing and exposure tool, could lead to sub-10 nm pitch resolution for this resist.

A manuscript entitled: "Resolution improvement for positive tone poly(methyl methacrylate) resist" is currently in preparation to be submitted in the next months. This manuscript includes the material previously explained in this thesis.

Annexes

Collaborations and Future Work

The work done in this thesis was as basic research for two different projects developed in the Quantum Nanostructures and Nanofabrication group at the Massachusetts Institute of Technology (MIT). In addition, I was involved in a third project during my stay, in the area of Helium Ion Milling of Graphene.

Finally, this section also presents the work on low-cost experiments on interference lithography, currently developed at the Electrochemistry and Chemical Energy Research Center (CELEQ) of the Universidad de Costa Rica.

A.1. Colloidal Quantum Dot Placement

This project was managed by Professor Karl Berggren from the Electrical Engineering and Computer Science (EECS) department in collaboration with Professor Moungi Bawendi from the Chemistry department both from MIT. The student in charge was Vitor R. Manfrinato and the work was supported by the Center for Excitonics, an Energy Frontier Research Center funded by the U.S. Department of Energy, Office of Science, Office of Basic Energy Sciences under Award Number DE-SC0001088.

The project demonstrated a technique to control the placement of CdSe and CdSe/CdZnS colloidal quantum dots (QDs) through electron-beam lithography. This technique fabricated sub-10 nm clusters of QDs. On average, each cluster had three dots, with a placement success rate of 87%. The controlled placement allowed positioning dots in close proximity, with a minimum separation of 12 nm[50].

This project performed photoluminescence (PL) measurements of the fabricated QD clusters, which showed that the dots continue to be optically active after the fabrication process, presenting intermittent PL as expected when doing measurements on clusters with a small number of QDs.

This collaboration project submitted its findings for review to the journal ACS Nano of the American Chemical Society, under the title "Controlled placement of colloidal quantum dots in sub-10-nm clusters"[44]. The contribution in this work is as one of the coauthors in the fabrication side of the project, not in the PL measurement process.

The work presented in this thesis provided a process to fabricate the smallest holes on PMMA to place individual QDs and to decrease the minimum separation of the QD clusters. Thus, the work looked towards increasing the resolution of double and triple dots structures for placement of QDs but it was expanded to study dot arrays and nested L's structures after obtaining promising results. In the same line, the Au/Ti lift-off was meant as a metrology strategy looking towards suitable templates for QD placement.

A.2. Templating of Protein Assemblies

This project was managed by Professor Karl Berggren and Professor Amy Keating from the Biology department of MIT. The postdoc in charge was Dr. Yong-Ho Kim. The project was funded by the International Iberian Nanotechnology Laboratory, under the specific project title of: "Top-Down Templating of Protein Assemblies: Complex Molecular Self-Assembly Routes to Biological Device Fabrication".

This project at the first steps looked towards guiding the placement of proteins by using Au posts as anchors to which the terminal tags of the proteins attached. The protein

used was cortexillin coiled-coils with a calculated length of 15 nm. The original project conception looked towards placing these coils between two Au posts and doing the necessary metrology to verify the proper controlled placement of the proteins. This project is still underway.

The contribution to this work was in making patterns with the sub-20 nm gaps needed between the Au posts for the protein attachment. The lift-off procedure shown in this thesis readily attained sub-20 nm gaps, therefore protein placement worked as a perfect first application of this high resolution patterning technique.

A.3. Helium Ion Milling of Graphene

This project was managed by Professor Karl Berggren, in collaboration with Professors Tomas Palacios and Jing Kong from the EECS department. The students in charge were Vitor R. Manfrinato and myself. This work was also collaboration with the Zeiss development plant in Peabody, Massachusetts, USA.

The work looked towards evaluating Zeiss' Orion Plus Helium Ion Microscope (HIM) as an etching tool for graphene nanoribbons (GNRs) and determining the edge roughness of the etching process, to look towards a better tool to develop high-resolution graphene devices. In addition, electrical measurements of the devices and graphene sheet resistance were intended, the latter by etching Hall bar structures in the material.

This project was successful from the nanofabrication side, etching and imaging 3.6 nm wide nanoribbons made from chemical vapor deposited graphene, and by learning how to optimize future grapheme etching processes with the HIM. These GNRs are one of the smallest imaged to date. Nonetheless, the fabrication process was not optimized for electrical measurements of the devices.

A.4. Low-cost Experiments on Interference Lithography

Interference lithography (IL) is a technology used to develop one- and two-dimensional periodic patterns (lines and dots arrays) on a substrate. This technique has great uses in several areas of materials science and engineering.

The CELEQ acquired an Archetto-3 IL system from Parian Technologies by using the budget from the 2012 Microstructures Research Center Fellowship (assigned to Jose P. Arrieta) and complementary funding from the CELEQ. The system is capable of resolving features with a periodicity ranging 203 and 600 nm and uses a GaN laser diode as the illumination source. Figure A-1 shows a schematic of the system acquired.

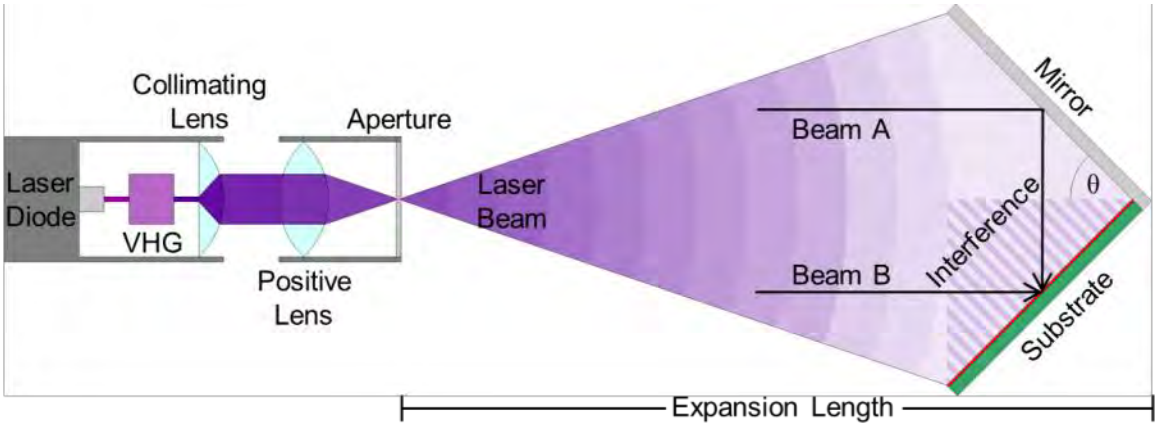

Figure A-1: Schematic of the Lloyd's Mirror interference lithography system acquired. In this configuration, laser illumination is emitted from a GaN (405 nm) laser diode, which passes through a variable holographic grating (VHG) stabilizing the output wavelength. The beam crosses a collimating lens that expands it. Afterwards the beam goes through a spatial filter, which focuses it on the aperture. The spatial filter removes nonuniformities of the beam, due to the lenses and the VHG. The beam leaves the aperture as a spherical wave, and after crossing the expansion length, the illumination propagates to form the equivalent of a plane, with parallel wave vectors. On the substrate, two contributions interfere with each other, one from the spatial filter and the other from the mirror, and form a one-dimensional standing wave, which exposes the resist layer.

The initial IL experiments intend to use low cost materials and metrology tools. In specific, the project uses water and sugar as base material, and metrology was done with crossed polarizers. This is done to determine the degree of orientation induced on the crystallization of the materials by the artificial one-dimensional and two-dimensional nanoscopic patterns (this process is known as graphoepitaxy), as a model experiment for future experiments in nanolithography. This project is still underway at the CELEQ.

Additionally, to expand the reach of this tool, the center is encouraging researchers in the university to use IL as an instrument in their scientific endeavors and developing processes-specific strategies to intended users of the tool.

Publication List

- **Arrieta, Jose P.**, Manfrinato, Vitor R., & Berggren, Karl K. (2012). Resolution improvement for positive tone poly(methyl methacrylate) resist. *Journal of Vacuum Science and Technology B*, *in preparation.*

- Manfrinato, Vitor R., Wanger, Darcy D., Strasfeld, David B., Han, Hee-Sun, Marsili, Francesco, **Arrieta, Jose P.**, Mentzel Tamar S., Bawendi Moungi G., & Berggren Karl K. (2012). Controlled placement of colloidal quantum dots in sub-15-nm clusters, *submitted.*

References

[1] Hoerni, J. A. (1959). *Patent No. 3025589*. United States of America.

[2] Buck, D. A., & Shoulders, K. R. (1959, July). An Approach to Microminiature Printed Systems. *Eastern Joint Computer Conference*, 55-59.

[3] Mack, C. A. (2011). Fifty Years of Moore's Law. *IEEE Transactions on Semiconductor Manufacturing, 24*(2), 202-207.

[4] Hewett, J. (2006). Immersion ideas extend optical lithography. *Optics & Laser Europe, 138*, 17-18.

[5] Pease, R. F. (2010). To charge or not to charge: 50 years of lithographic choices. *Journal of Vacuum Science & Technology B, 28*(6), C6A1-C6A6.

[6] Arnold, C. B., Serra, P., & Piqué, A. (2007). Laser Direct-Write Techniques for Printing of Complex Materials. *MRS Bulletin, 32*(01), 23-31.

[7] Liu, G.-Y., Xu, S., & Qian, Y. (2000). Nanofabrication of Self-Assembled Monolayers Using Scanning Probe Lithography. *Accounts of Chemical Research, 33*(7), 457-466.

[8] McCord, M. A., & Pease, R. F. (1986). Lithography with the scanning tunneling microscope. *Journal of Vacuum Science and Technology B, 4*(1), 86-88.

[9] Smith, H. I. (1996). A proposal for maskless, zone-plate-array nanolithography. *Journal of Vacuum Science and Technology B, 14*(6), 4318-4322.

[10] Wells, O. C., Everhart, T. E., & Matta, R. K. (1965). Automatic positioning of device electrodes using the scanning electron microscope. *Electron Devices, IEEE Transactions on, 12*(10), 556-563.

[11] Broers, A. N., & Lean, E. G. (1969). 1.75 GHz Acoustic-surface-wave Transducer Fabricated by an Electron Beam. *Applied Physics Letters, 15*(3), 98-101.

[12] Rishton, S. A., & Kern, D. P. (1987). Point exposure distribution measurements for proximity correction in electron beam lithography on a sub-100 nm scale. *Journal of Vacuum Science and Technology B, 5*, 135-141.

[13] Duan, H., Winston, D., Yang, J. K., Cord, B. M., Manfrinato, V. R., & Berggren, K. K. (2010). Sub-10-nm half-pitch electron-beam lithography by using poly(methyl methacrylate) as a negative resist. *Journal of Vacuum Science and Technology B, 28*, C6C58-C6C62.

[14] Cui, Z. (2005). *Micro- Nanofabrication Technologies and Applications*. Beijing: Higher Education Press, Springer-Verlag.

[15] Cui, Z. (2008). *Nanofabrication Principles, Capabilities and Limits*. New York: Springer Science + Business Media.

[16] Mack, C. A. (2008). *Fundamental Principles of Optical Lithography, The Science of Microfabrication*. West Sussex: John Wiley & Sons Ltd.

[17] Cabrini, S., & Kawata, S. (2012). *Nanofabrication Handbook*. Boca Raton: CRC Press.

[18] Orloff, J. (2009). *Handbook of Charged Particles Optics*. Boca Raton: CRC Press.

[19] van Dorp, W. F., van Someren, B., Hagen, C. W., & Kruit, P. (2005). Approaching the Resolution Limit of Nanometer-Scale Electron Beam-Induced Deposition. *Nano Letters*, 5(7), 1303-1307.

[20] Yang, J. K., & Berggren, K. K. (2007). Using high-contrast salty development of hydrogen silsesquioxane for sub-10-nm half-pitch lithography. *Journal of Vacuum Science and Technology B, 25*, 2025-2029.

[21] Grigorescu, A. E., van der Krogt, M. X., Hagen, C. W., & Kruit, P. (2007). 10 nm lines and spaces written in HSQ, using electron beam lithography. *Microelectronic Engineering, 84*(5-8), 822-824.

[22] Manfrinato, V. R., Zhang, L., Su, D., Duan, H., Stach, E. A., & Berggren, K. K. (2012). Resolution limits of electron-beam lithography towards the atomic scale. *in preparation*.

[23] van Oven, J. C., Berwald, F., Berggren, K. K., Kruit, P., & Hagen, C. W. (2011). Electron-beam-induced deposition of 3-nm-half-pitch patterns on bulk Si. *Journal of Vacuum Science and Techhnology B, 29*, 06F305.

[24] Bita, I., Yang, J. K., Jung, Y. S., Ross, C. A., Thomas, E. L., & Berggren, K. K. (2008). Graphoepitaxy of Self-Assembled Block Copolymers on Two-Dimensional Periodic Patterned Templates. *Science, 321*(5891), 939-943.

[25] Tavakkoli K.G., A., Gotrik, K. W., Hannon, A. F., Alexander-Katz, A., Ross, C. A., & Berggren, K. K. (2012). Templating Three-Dimensional Self-Assembled Structures in Bilayer Block Copolymer Films. *Science, 336*(6086), 1294-1098.

[26] Chen, Z., Lin, Y.-M., Rooks, M. J., & Avouris, P. (2007). Graphene nano-ribbon electronics. *Physica E, 40*(2), 228-232.

[27] Daves, W., Ruoff, M., Fleischer, M., Wharam, D. A., & Kern, D. P. (2010). Hydrogen silsesquioxane electron beam lithography for ultra-small single electron transistors in silicon on insulator. *Microelectronic Engineering, 87*(5-8), 1643-1645.

[28] Terris, B. D. (2009). Fabrication challenges for patterned recording media. *Journal of Magnetism and Magnetic Materials, 321*(6), 512-517.

[29] Yang, J. K., Chen, Y., Huang, T., Duan, H., Thiyagarajah, N., Hui, H., et al. (2011). Fabrication and characterization of bit-patterned media beyond 1.5 Tbit/in2. *Nanotechnology, 22*(38).

[30] Wu, W., Tong, W. M., Bartman, J., Chen, Y., Walmsley, R., Yu, Z., et al. (2008). Sub-10 nm Nanoimprint Lithography by Wafer Bowing. *Nano Letters, 8*(11), 3865-3869.

[31] Austin, M. D., Ge, H., Wu, W., Li, M., Yu, Z., Wasserman, D., et al. (2004). Fabrication of 5 nm linewidth and 14 nm pitch features by nanoimprint lithography. *Applied Physics Letters, 84*(26), 5299-5301.

[32] Haller, I., Hatzakis, M., & Srinivasan, R. (1968). High-resolution Positive Resists for Electron-beam Exposure. *IBM Journal of Research and Development, 12*(3), 251-256.

[33] Arjmandi, N., Lagae, L., & Gustaaf, B. (2009). Enhanced resolution of poly(methyl methacrylate) electron resist by thermal processing. *Journal of Vacuum Science and Technology B, 27*, 1915-1918.

[34] Dial, O., Cheng, C. C., & Scherer, A. (1998). Fabrication of high-density nanostructures by electron beam lithography. *Journal of Vacuum Science and Technology B, 16*, 3887-3890.

[35] Broers, A. N., Hoole, A. C., & Ryan, J. M. (1996). Electron beam lithography—Resolution limits. *Microelectronic Engineering, 32*(1-4), 131-142.

[36] Craighead, H. G. (1984). 10-nm resolution electron-beam lithography. *Journal of Applied Physics, 55*(12), 4430-4435.

[37] Vieu, C., Carcenac, F., Pépin, A., Chen, Y., Mejias, M., Lebib, A., et al. (2000). Electron beam lithography: resolution limits and applications. *Applied Surface Science, 164*(1-4), 111-117.

[38] Beaumont, S. P., Bower, P. G., Tamamura, T., & Wilkinson, C. D. (1981). Sub-20-nm-wide metal lines by electron-beam exposure of thin poly(methyl methacrylate) films and liftoff. *Applied Physics Letters, 38*(6), 436-439.

[39] Cord, B. M., Lutkenhaus, J., & Berggren, K. K. (2007). Optimal temperature for development of poly(methylmethacrylate). *Journal of Vacuum Science and Technology B*, 2013-2016.

[40] Novotny, L., & van Hulst, N. (2011). Antenas for light. *Nature Photonics, 5*, 83-90.

[41] Duan, H., Hu, H., Kumar, K., Shen, Z., & Yang, J. K. (2011). Direct and Reliable Patterning of Plasmonic Nanostructures with Sub-10-nm Gaps. *ACS Nano, 5*(9), 7593-7600.

[42] Lal, S., Link, S., & Halas, N. J. (2007). Nano-optics from sensing to waveguiding. *Nature Photonics, 1*, 641-648.

[43] Duan, H., Fernández-Dominguez, A., Bosman, M., Maier, S. A., & Yang, J. K. (2012). Nanoplasmonics: Classical down to the Nanometer Scale. *Nano Letters, 12*(3), 1683-1689.

[44] Manfrinato, V. R., Wanger, D., Strasfeld, D., Han, H. -S., Marsili, F., Arrieta, J. P., et al. (2012). Controlled placement of colloidal quantum dots in sub-15-nm clusters. *Nano Letters, submitted.*

[45] Abramson, J.J., Palma, M., Wind, S. J., & Hone, J. (2012). Quantum Dot Nanoarrays: Self-Assembly With Single-Particle Control and Resolution. *Advanced Materials, 24*(16), 2207-2211.

[46] Chai, J., Wong, L. S., Giam, L., & Mirkin, C. A. (2011). Single-molecule protein arrays enabled by scanning probe block copolymer lithography. *Proceedings of the National Academy of Sciences of the United States of America, 108*(49), 19521-19525.

[47] Goodberlet, J. G., Hastings, T., & Smith, H. I. (2001). Performance of the Raith 150 electron-beam lithography system. *Journal of Vacuum Science and Technology B, 19*, 2499-2503.

[48] Duan, H., Manfrinato, V. R., Yang, J. K., Winston, D., Cord, B. M., & Berggren, K. K. (2010). Metrology for electron-beam lithography and resist contrast at the sub-10 nm scale. *Journal of Vacuum Science and Technology B, 28*, C6H11-C6H17.

[49] Yang, J. K., Cord, B. M., Duan, H., Berggren, K. K., Klingfus, J., Nam, S.-W., et al. (2009). Understanding of hydrogen silsesquioxane electron resist for sub-5-nm-half-pitch lithography. *Journal of Vacuum Science and Technology, 27*, 2622-2627.

[50] Manfrinato, V. R. (2011). Sub-10-nm electron-beam lithography for templated placement of colloidal quantum dots. *MIT M. Sc. Thesis.*